**Multidisciplinary Optimization Standardization Approach for Integration and Configurability**
***MOSAIC Project***

## Task 6

# WING–BOX STRUCTURAL DESIGN OPTIMIZATION

# Report 5

## Wing Rib Stress Analysis and Design Optimization

**By**

Ramin Sedaghati, Ph.D, P.Eng.
Associate Professor
Principle Investigator for Task 6

Mostafa S.A. Elsayed, M.Sc.
Ph.D. student

Department of Mechanical and Industrial Engineering
Concordia University

**Sponsor's Ref. No: CRIAQ 4.1-TASK 6**

**June 2006**

# ***Wing Rib Stress Analysis and Design Optimization***


## ***Abstract***

For aerodynamic reasons the wing contours in the chord wise direction must be maintained without appreciable distortion. Therefore, to hold the skin-stringer wing surface to contour shape and also to limit the length of the stringers to an efficient column compressive length, internal supporting units are required. These supporting units are referred to as wing ribs.

In the current report, a complete stress analysis for a wing rib subjected to different kinds of loading is introduced. Two methodologies for the design of the wing rib are presented. The first method is designing the wing rib as a shear resistant plate girder that will not buckle nor yield under the applied loads. This method is used for the design of the lightly loaded ribs where the web stiffeners are omitted and instead a series of standard flanged lightening holes are introduced. The second method presents a methodology for the design of a wing rib subjected to moderate to heavy loads (bulkheads). The second method is based on the incomplete diagonal tension theory. Designing a rib subjected to heavy loads to act as a shear resistant plate girder will produce a very massive rib. Instead the thickness of the rib will be reduced to the limit to keep it within the elastic deformations limit but with less buckling resistibility where the rib is forced to be under incomplete diagonal tension field stresses. Uprights are introduced to the rib to support rib buckling. A complete stress analysis for the wing rib as well as web uprights is presented. The analysis procedure is based on theoretical evidence as well as empirical formulations.



## ***Key Words***

Wing-Box, Skin-Stringer Panels, Ribs and Spars, Maximum Shear Flow, Diagonal Tension, Incomplete Diagonal Tension, Multi Disciplinary Design Optimization (MOD).

# ***Table of Contents***

## ***List of Figures***

## ***List of Tables***

# *Section I Overview*

## *I-1 Description of the Project:*

The objective of task 6 in the MOSAIC project is to improve the available structural analysis modules in the Bombardier Aerospace and perform a structural design optimization of the wing box by adding an optimization loop around the analysis code. The objective is to design a wing-box more rapidly and automatically. Task 6 is divided into four stages.

### *Stage I: Optimization of one skin stringer panel:* (finished)

Stage I explained in details the procedure to optimize one skin-stringer panel consists of one stringer with one stringer spacing (or pitch) of skin in the chord wise direction and the distance between two ribs in the span wise direction. Skin-stringer panels on the upper and lower wing covers are considered. The load acting on the panels is taken to be constant (i.e. same load acting on all panels) which resulted in identical dimensions for all panels. Stage-I provides a methodology to obtain the optimum dimensions for a skin-stringer compression panel with a minimum mass under six constraints namely crippling stress, column buckling, up-bending at center span (compression in skin), down-bending at supports (compression in stringer outstanding flange), inter-rivet buckling and beam column eccentricity. It also provides optimum design variables for panels under tensile loading with fatigue life as a design constraint with same objective function (Minimum mass for panel). A panel on the lower wing cover is designed for Damage Tolerance. (For more details refer to report II and III)

### *Stage II: Load Redistribution:* (Finished)

Stage II presented the methodology for calculating the actual load experienced by each skin-stringer panel when arranged on the airfoil profile at any span wise section of the wing. The number of stringers required on the upper and lower wing covers is obtained by dividing the width of the wing-box by their corresponding stringer pitch obtained from stage I. These panels are then re-

arranged on the actual airfoil profile at certain span wise section. Each panel now experiences different magnitude of compressive or tensile load depending on its relative location with respect to the centriodal axes of the section.
The optimum dimensions for panels on upper and lower wing covers are thus obtained using stage-I optimization program with the new calculated design load which resulted in a different optimum dimensions for each panel according to its location. (For more details refer to report IV).

***Stage III: Optimization of the Spars and Spar Caps:*** (In progress)

This stage is an extension to stage II. In this stage the development of the optimization tools to include the spars thickness and web cap dimensions will be considered.

***Stage IV: FE Model of the wing box:*** (In Progress)

After all components are optimally sized, the FE model of the wing box will be developed in order to find the stress and deflection distribution and evaluate margins of safety. The model is being developed using NASTRAN 2005.1 environment.

The optimization processes of the four stages are being tested on theDLR-F6 aircraft wing box.

## *I-2 DLR-F6 Aircraft Geometry and Wing Details:*

The geometry and load details are taken from DLR-F6 aircraft [1]. The actual wind tunnel model geometry is shown in Figure (1).
Axes x, y and z denote the coordinate system for the aircraft body and axes x*, y* and z* refer to the wing coordinate system. The wing with nacelle is defined in wing coordinate system and is placed in the body system (according to Figure (1)) with x and z translations of 13.661 in. and -1.335 in respectively with a dihedral of 4.787 degrees.

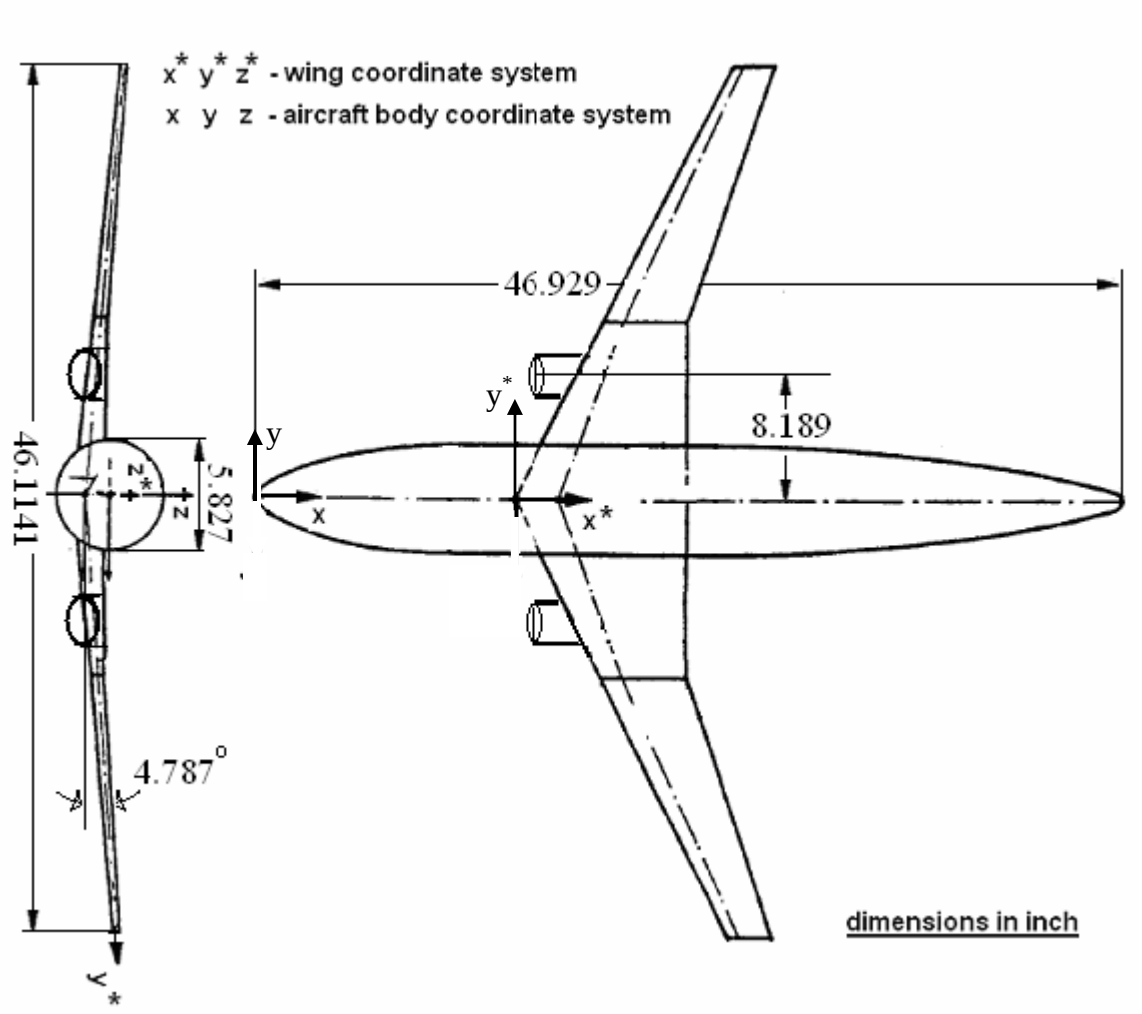


Fig. (1) DLR-F6 wind tunnel model geometry [1]

The nacelle is located at 8.189 in. from the wing origin. The projected wing semi-span is 23.0571 in. The wing is defined by a number of airfoil sections at different stations along the wing span as shown in Figure (2). The shape of the airfoil at each station is selected based on the aerodynamics and holds the shape of the wing.

In order to test the optimization, the wind tunnel geometry is scaled by a factor λ=20 to build an approximately realistic aircraft model. The scaled model dimensions of the wing are given below:

The wing reference area for the scaled model is S=90148 $in.^2$ and the semi-span in wing coordinate system is $s^*$= 463.3 in. The average chord length of the wing is $C_{av} = 97.746$ in. and the mean aerodynamic chord length is $C_{mac} = 111.18$ in.

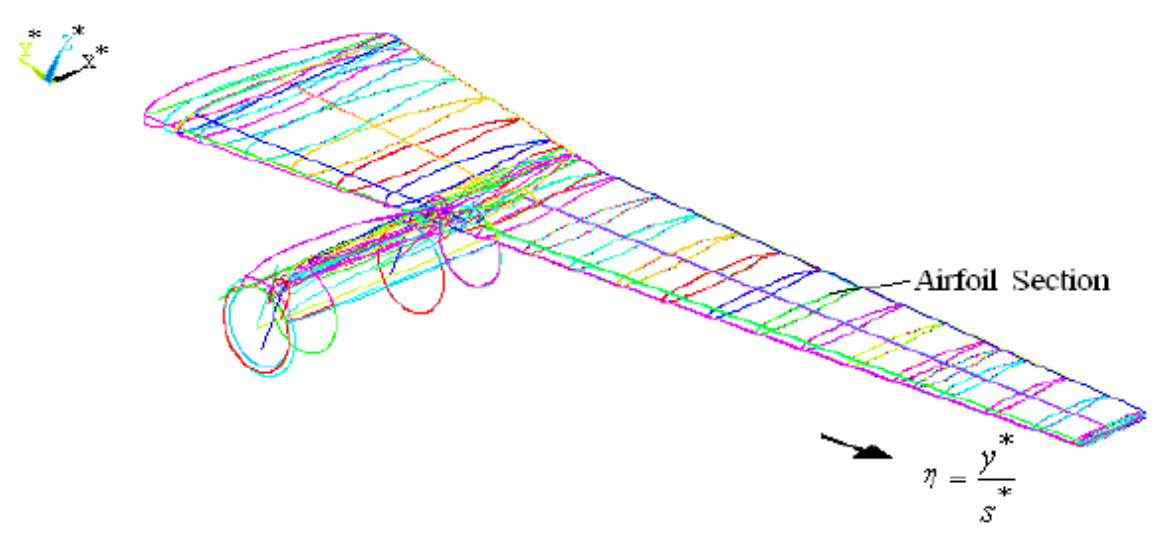


Fig. (2) DLR-F6 wing showing different airfoil sections [1]

Figure (2) a number of airfoil sections that are defined at different η along the wing span, where η is the normalized coordinate defined as $\eta = \frac{y^*}{s^*}$ .

The front spar is usually positioned at 15% of chord and the rear spar at 65% of chord measured from the leading edge. The enclosed area between the spars as shown is called the wing-box.

# Section II Wing Rib Stress Analysis

## II-1 General:

The aircraft is constructed primarily from thin metal skins which are capable of resisting in plane tension and shear loads but buckle under comparatively low values of in-plane compressive loads. The skin therefore is stiffened by longitudinal stringers which resist the in-plane compressive loads and at the same time resist small distributed loads normal to the plan of the skin. For aerodynamic reasons the wing contours in the chord wise direction must be maintained without appreciable distortion. Therefore to hold the skin-stringer wing surface to contour shape internal structural support units are presented which are referred to as wing ribs.

Figure (3) shows the internal construction of the historical aircraft 727, where the lower skin is not installed, showing the wing ribs between the lower and the front spars and their extension in the leading edge.

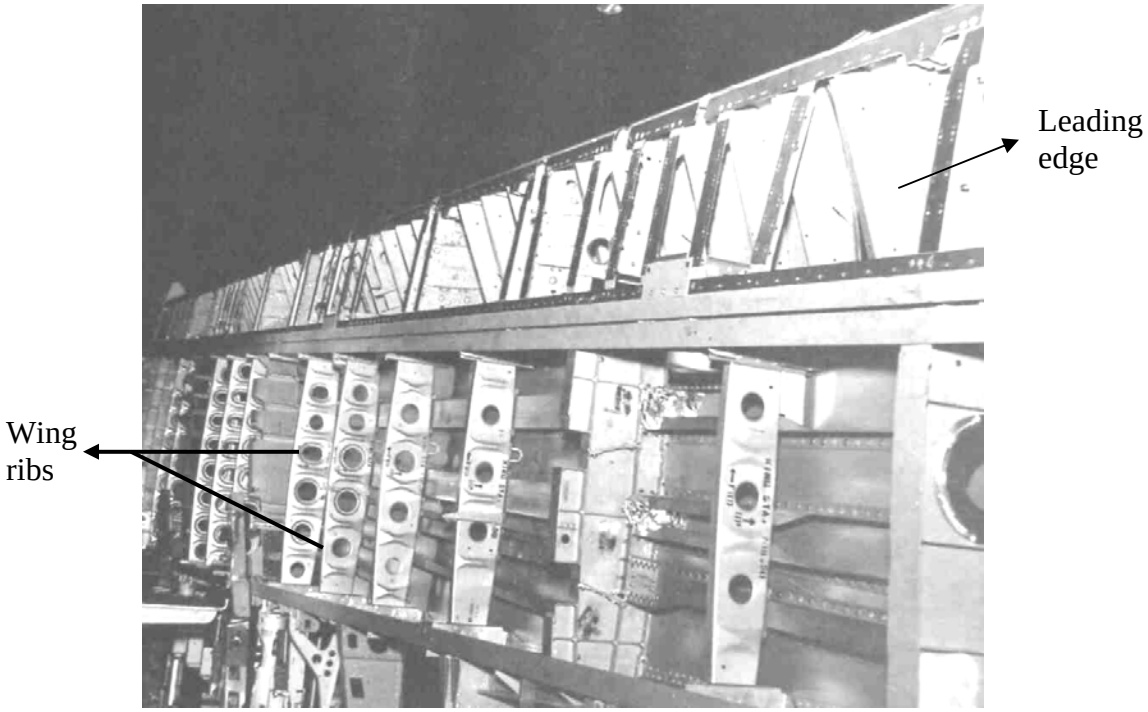


Fig. (3) 727 aircraft wing with lower skin not installed showing the wing ribs [3]

In addition to the wing rib main function of maintaining the wing aerodynamic shape, the ribs also are presented for many other purposes that can be summarized as:

1- Limiting the length of the stringers to an efficient column compressive strength which increases the skin-stringers stability under compressive loads.
2- Transferring and distribution loads

All the loads applied to the wing are reacted at the wing supporting points, thus these applied loads must be transferred into the wing cellular structure composed of skin, stringers spars,…etc and then react at the wing supporting points, these applied loads can be summarized as

a- Aerodynamic loads acting on the skin-stringer panels are transferred to the rib webs, which by its roll transfer it to the spars. this function requires light ribs.
b- Concentrated forces resulting from landing gears and power plants support points. These forces should be transferred to the wing cellular units in the form of distributed shear flows, this function is handled by the wing ribs which requires heavy ribs referred to as bulkheads.
c- Between the forces mentioned in 'a' and 'b' there are medium forces resulting from the flaps, ailerons, fuel tanks supporting points, armaments,…etc.
d- Body forces in the form of gravitational forces (wing structural weight) and inertia forces due to wing structural mass.

3- Redistributing shear forces at discontinuities in the wing in the form of cutouts for the landing gears, inspection holes, …etc.

## ***II-2 Construction of the Wing Rib:***

The wing rib extends from the leading edge to the trailing edge of the aircraft wing, thus it can be divided into three main parts namely the leading and the trailing edges rib portions and the wing box rib portion. Between the three

portions, the front and the rear spars are accommodated where the rib is riveted into its webs, as shown in Figure 4.

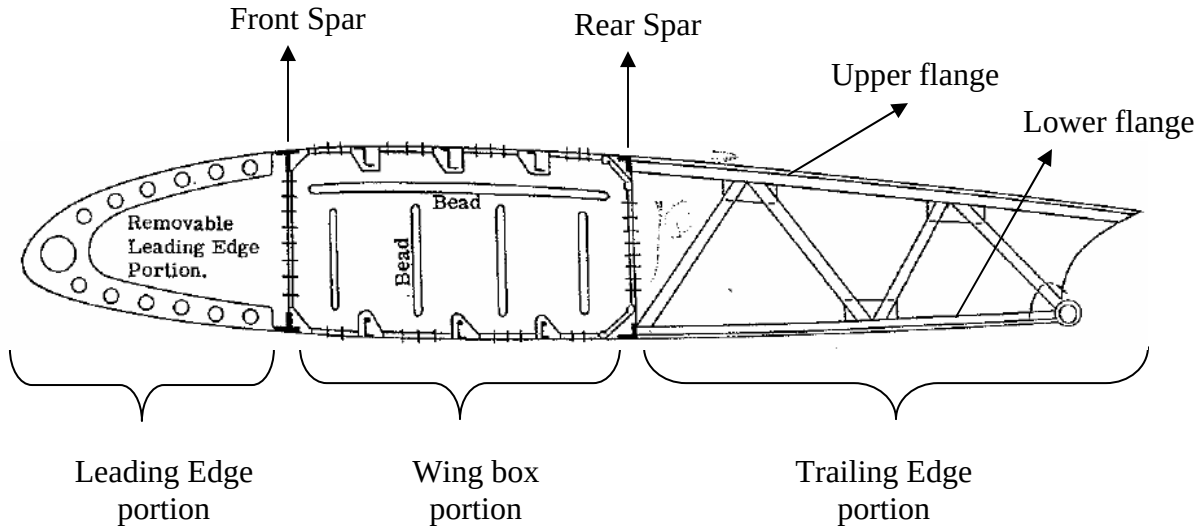


Fig. (4) Wing rib Construction [3]

The assembly of the rib with the wing skin-stringer panels has different configurations. The rib may be riveted, spot welded or glued to the skin along its boundary as shown in figure (5).

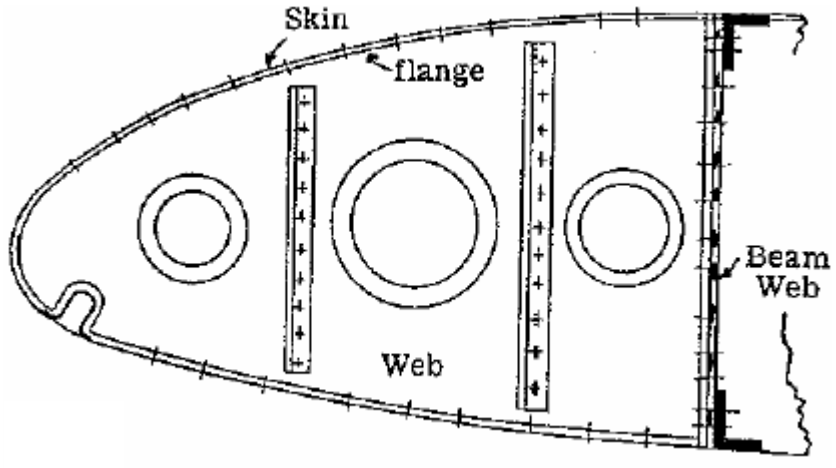


Fig. (5) Leading edge wing rib- skin assembly by riveting [3]

In some other cases the rib is notched to host the stringers, as shown in Figure 6 where the lower flange of the rib is notched to host the stringers of the lower skin.

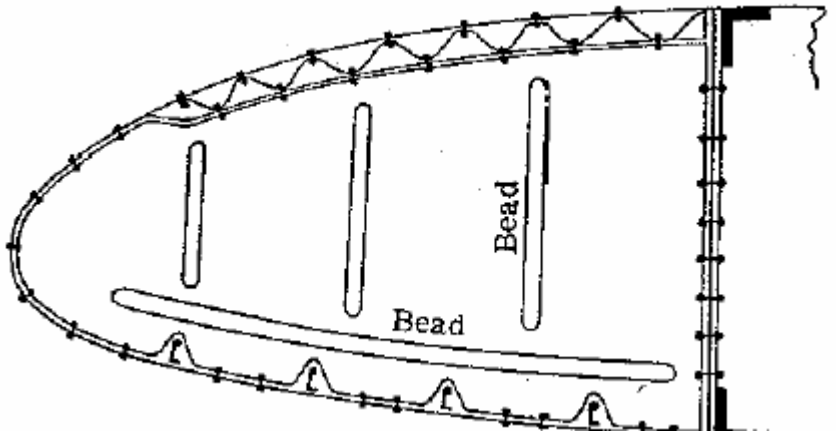


Fig. (6) Leading edge wing rib- skin assembly [3]

Lightening holes may be introduced to the web of the rib for mass reduction, accessibility and to form a passage for wiring and fuel pipes. Different kinds of ribs and different rib assemblies are required in the aircraft design. Since the ribs compose an appreciable part of the wing, an accurate design for the wing rib that guarantee the necessary strength with minimum weight.

In the current report, a complete stress analysis for a wing box rib portion subjected to different kinds of loading is introduced. Two methodologies for the design of the wing rib are presented. The first method is designing the wing rib as a shear resistant plate girder that will not buckle nor yield under the applied loads. This method is used for the design of the lightly loaded ribs where the web stiffeners are omitted and instead a series of standard flanged lightening holes are introduced. The second method presents a new methodology for the design of the wing rib subjected to moderate to heavy loading (bulkheads). This method is based on the incomplete diagonal tension theory where the rib is forced to be under incomplete diagonal tension field. Uprights are introduced to the rib to support rib buckling. A complete stress analysis for the wing rib as well as web uprights is presented. The analysis procedure is based on theoretical evidence supported by empirical formulations. While the third method is a survey on the

design methodology suggested by Paul Kuhn, et.al. in their report 'Summary of Diagonal Tension- Part One, NACA Technical Note 2661' [7].

## ***II-3 Loads Acting on the Wing Rib:***

As mentioned before, the wing rib is mainly subjected to three kinds of loading

a) Aerodynamic loads transmitted from the skin-stringer wing panels.
These aerodynamic loads include lift force, drag force, pitching moment, and stringers axial forces components in the rib plane (due to stringer inclination in tapered sections).
b) Concentrated forces transmitted to the rib due to landing gear connections, power plant's nacelle connections, connections to the fuselage, connection with the controlling surfaces structures like ailerons…etc.
c) Body forces in the form of gravitational forces and inertia forces due to wing structural mass.

The stress analysis of the wing rib requires a complete identification of all the loads acting on its structure.

## ***II-3-1 Aerodynamic Loads:***

Generally, an aircraft flying in air is subjected to aerodynamic loads [2, 3]. The lift produced by the aircraft balances its weight and the drag force balances the thrust produced by the aircraft as shown in Figure (7).

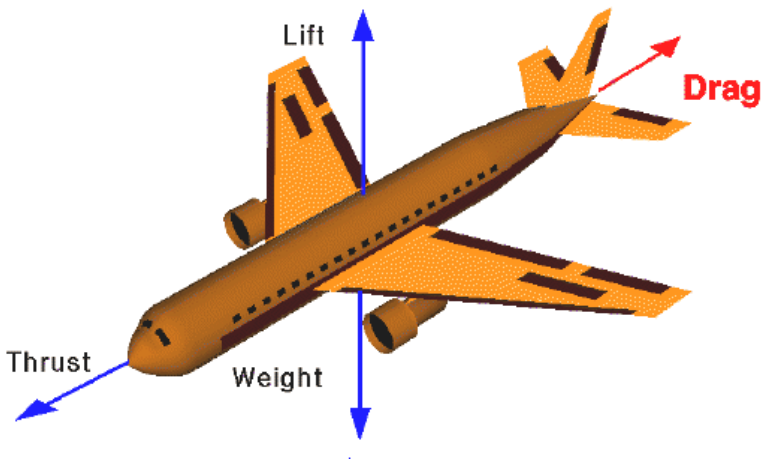


Fig. (7) Lift & Weight and Drag & Thrust balancing the Aircraft [1]

Figure (8) shows different rotational motions exhibited by an aircraft. Pitching moment is expressed about the center of gravity of the aircraft.

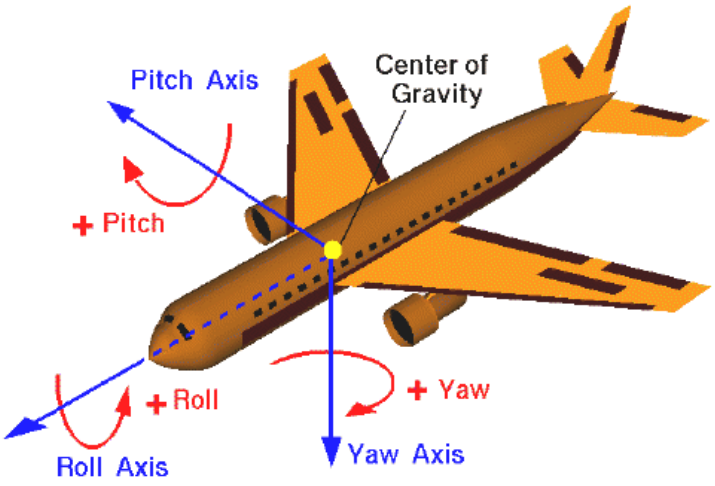


Fig. (8) Pitch, Yaw and Roll motions of an Aircraft [1]

The loads experienced by an aircraft wing are usually expressed in terms of aerodynamic coefficients [2], namely, the lift coefficient ($C_L$), the drag coefficient ($C_D$), the pitching moment coefficient ($C_M$), the normal force coefficient ($C_N$) and the tangential force coefficient ($C_T$). All these coefficients are usually calculated by wind tunnel tests since testing an actual aircraft is quite cumbersome and expensive. The above coefficients are all defined as below:

$$C_L = \frac{L}{q_\infty S} \tag{1}$$

$$C_D = \frac{D}{q_\infty S} \tag{2}$$

$$C_M = \frac{M}{q_\infty S c} \tag{3}$$

$$C_N = \frac{N}{q_\infty S} \tag{4}$$

$$C_T = \frac{T}{q_\infty S} \tag{5}$$

Where $S$ is the wing reference area; for airfoils a reference length is required rather than an area; thus the chord or length of the airfoil section is used for this purpose. $q_\infty$ is the free stream dynamic pressure calculated as:

$$q_\infty = \frac{1}{2}\rho V^2 \tag{6}$$

Where $\rho$ and $V$ are the density of air and speed of the aircraft (calculated from Mach number, $M$) respectively. Since the speed of sound varies with the density of air, it is required to determine the density of the air through which the aircraft is flying. To compute this, the chart shown in Table (1), called the International Civil Aviation Organization Table (ICAO) is always used. It can be noticed that as the altitude increases, the density of air decreases and so does the speed of sound.

Table 1: Variation of density of air and speed of sound with altitude

| **Altitude (*ft*)** | **Density of Air ($kg/m^3$)** | **Speed of Sound ($m/s$)** |
|---|---|---|
| 0 | 1.2249 | 340.4076 |
| 1000 | 1.1894 | 339.2758 |
| 2000 | 1.1548 | 338.0926 |
| 3000 | 1.1208 | 336.9094 |
| 4000 | 1.0878 | 335.7262 |
| 5000 | 1.0554 | 334.5429 |
| 6000 | 1.0239 | 333.3083 |
| 7000 | 0.9930 | 332.1250 |
| 8000 | 0.9626 | 330.9418 |
| 9000 | 0.9332 | 329.7072 |
| 10000 | 0.9044 | 328.5239 |
| 15000 | 0.7709 | 322.4021 |
| 20000 | 0.6524 | 316.1773 |
| 25000 | 0.5488 | 309.7982 |
| 30000 | 0.4581 | 303.2647 |
| 35000 | 0.3798 | 296.6284 |
| 40000 | 0.3015 | 295.1880 |
| 45000 | 0.2370 | 295.1880 |
| 50000 | 0.1865 | 295.1880 |
| 55000 | 0.1469 | 295.1880 |

When a wind tunnel is used to collect aerodynamic data, first the actual lift force $L$ *is measured* then it is converted to a non-dimensional coefficient $C_L$ using equation (1). All the complex aerodynamics has been hidden away in the lift coefficient. It is noticed that $C_L$ depends on the angle of attack ($\alpha$), Mach number (M) and Reynolds's number (Re). To summarize, the lift coefficient it becomes a function of three variables,

$$C_L = f(\alpha, \mathrm{M}, Re) \tag{7}$$

The CFD solution for wing-body-pylon-engine (wing-mounted engine) case giving the lift coefficient and pitching moment coefficient for DLR-F6 aircraft wing at test conditions of Mach = 0.75; CL=0.5 (CL is the overall lift coefficient); $\alpha = -0.0111^{o}$ and $Re = 0.300E7$ is given in Tables (2) and (3).

Table 2 Variation of Lift Coefficient (vs) $\eta$

| $\eta = \frac{y^*}{s^*}$ | $C_L$ | $c$ |
|---|---|---|
| 0.1274 | 0.4328 | 158.8756 |
| 0.1651 | 0.4580 | 149.9319 |
| 0.2029 | 0.4784 | 140.9653 |
| 0.2409 | 0.4908 | 131.9525 |
| 0.2793 | 0.4926 | 122.8697 |
| 0.3180 | 0.4864 | 113.6916 |
| 0.3572 | 0.5141 | 104.3917 |
| 0.3971 | 0.5483 | 94.9413 |
| 0.4377 | 0.5698 | 91.3885 |
| 0.4792 | 0.5899 | 88.1641 |
| 0.5219 | 0.6068 | 84.8560 |
| 0.5657 | 0.6212 | 81.4495 |
| 0.6111 | 0.6340 | 77.9280 |
| 0.6582 | 0.6439 | 74.2717 |
| 0.7074 | 0.6502 | 70.4573 |
| 0.7589 | 0.6553 | 66.4566 |
| 0.8133 | 0.6504 | 62.2348 |
| 0.8711 | 0.6353 | 57.7487 |
| 0.9330 | 0.5861 | 52.9427 |
| 1.0000 | 0.4832 | 47.7443 |

Tables (2) shows the variation of the local lift coefficient at different stations along the wing span where "$C_L$" is the local lift coefficient at a specific span coordinate and "$c$" is the local chord length at that span coordinate.

Figure (9) shows the variation of the lift coefficient along the wing span. From table (2) and by using equation (1), the lift force per unit length along the wing span can be calculated, as shown in figure (10).

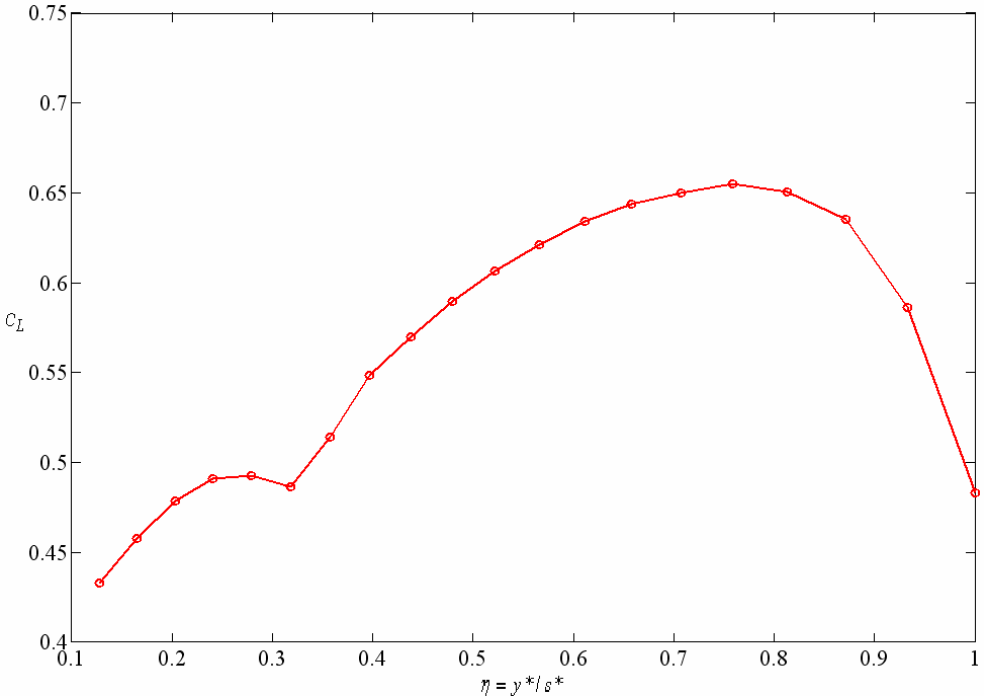


Fig. (9) $C_L$ (vs) $\eta$

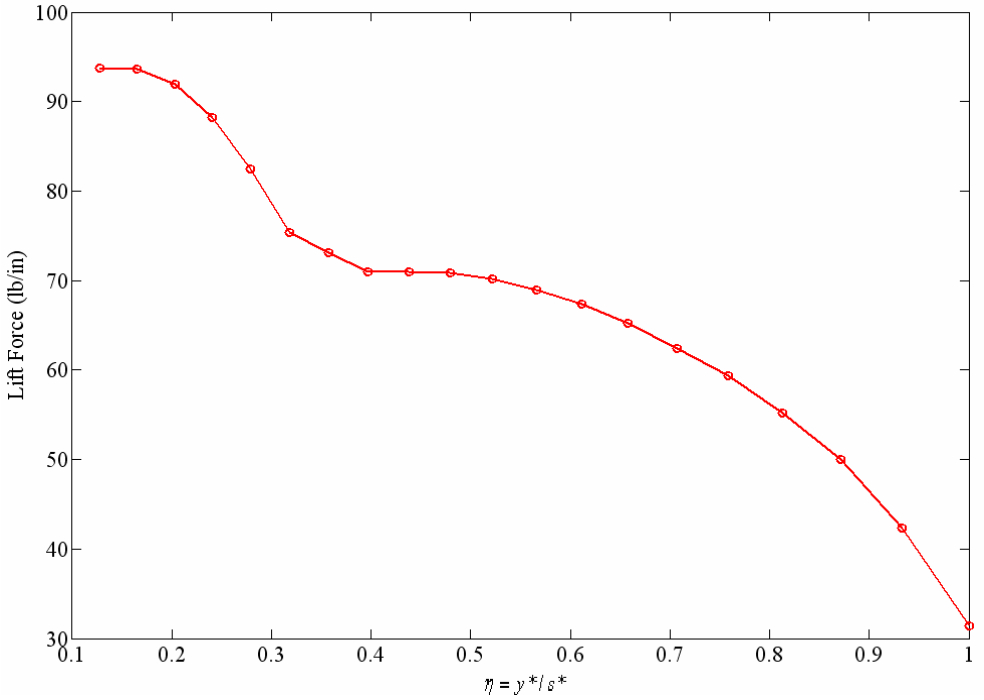


Fig. (10) Lift Force per unit length (vs) $\eta$

Table (3) Pitching Moment Coefficient about Local Quarter Chord (vs) $\eta$

| $\eta = \frac{y^*}{s^*}$ | $C_{Mqc}$ |
|---|---|
| 0.1274 | -0.0958 |
| 0.1651 | -0.0929 |
| 0.2029 | -0.0939 |
| 0.2409 | -0.0987 |
| 0.2793 | -0.1071 |
| 0.3180 | -0.1201 |
| 0.3572 | -0.1374 |
| 0.3971 | -0.1461 |
| 0.4377 | -0.1381 |
| 0.4792 | -0.1325 |
| 0.5219 | -0.1280 |
| 0.5657 | -0.1249 |
| 0.6111 | -0.1231 |
| 0.6582 | -0.1221 |
| 0.7074 | -0.1228 |
| 0.7589 | -0.1222 |
| 0.8133 | -0.1203 |
| 0.8711 | -0.1165 |
| 0.9330 | -0.1128 |
| 1.0000 | -0.1093 |

Table (3) shows the values of pitching moment coefficient about quarter chord length along the wing span. These data are represented graphically in Figure (11). From table (3) and by using equation (3), the pitching moment about quarter chord length can be calculated, as shown in Figure (12).

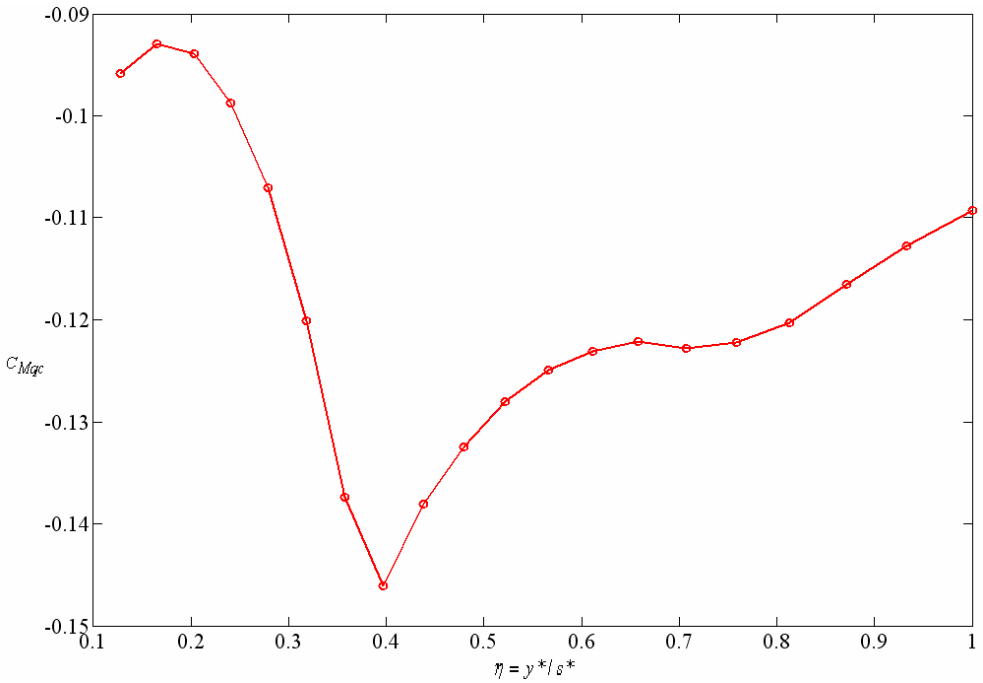


Fig. (11) $C_{Mqc}$ (vs) $\eta$

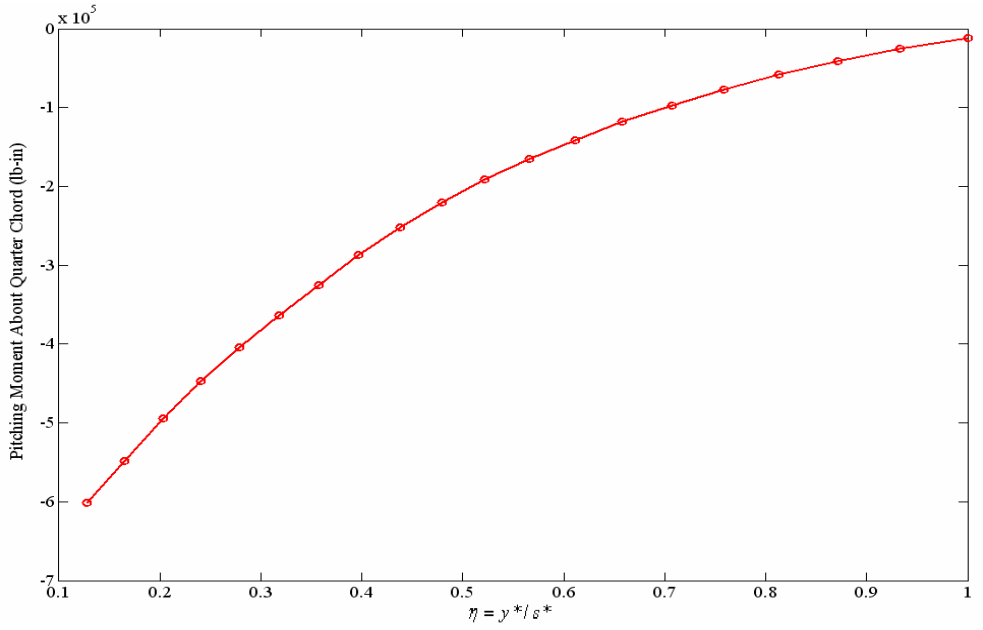


Fig.(12) Total Pitching Moment (about Quarter Chord) (vs) $\eta$

Integration of the curve in Figure 10 along the spanwise direction gives the shear force distribution on the wing as shown in Figure 13. The bending moment distribution along the wing span can also be obtained by integrating the shear force distribution as shown in Figure (14).

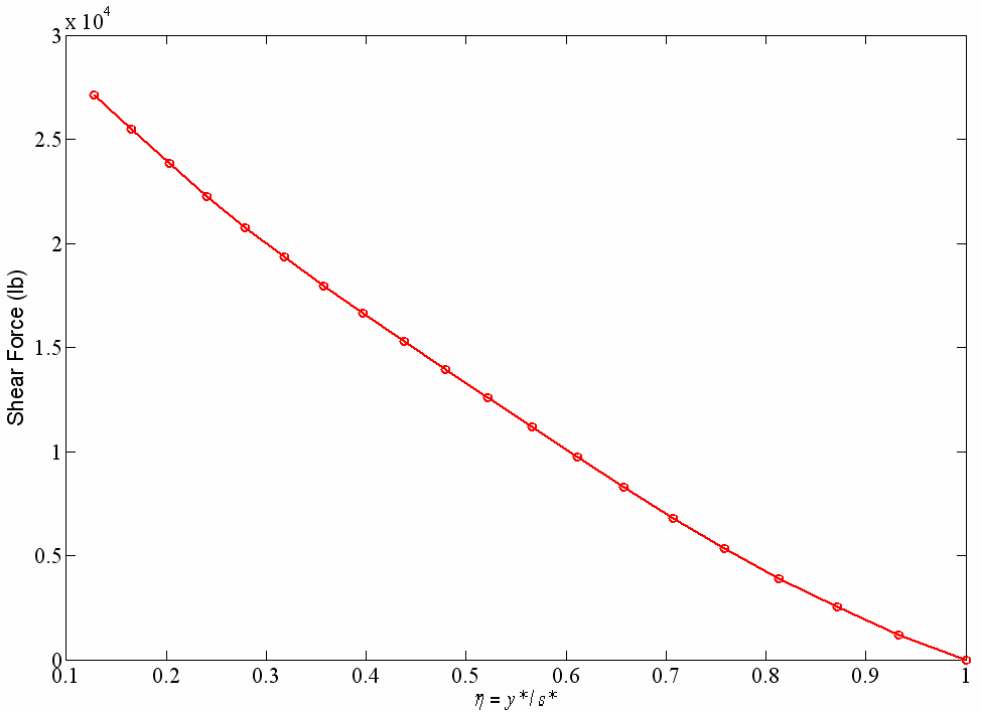


Fig. (13) Shear Force (vs) $\eta$

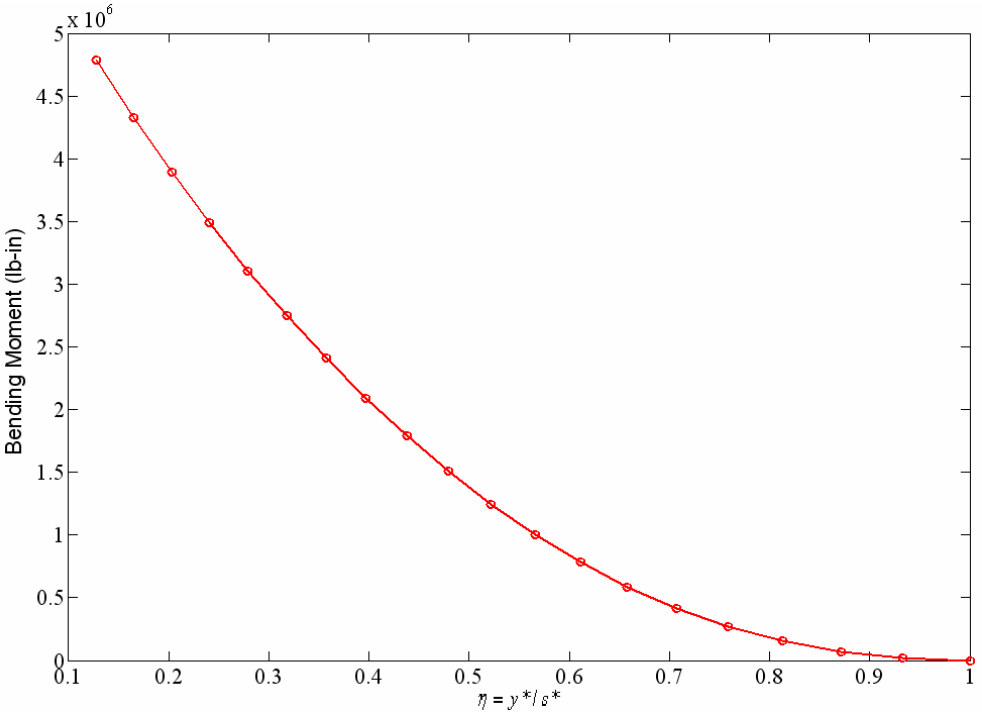


Fig. (14) Bending moment (vs) $\eta$

It is important to mention that the lift force is also varying in the chordwise direction as well as its variation along the wing span, due to the aerodynamic pressure variation along the chord as shown in Figure (15).

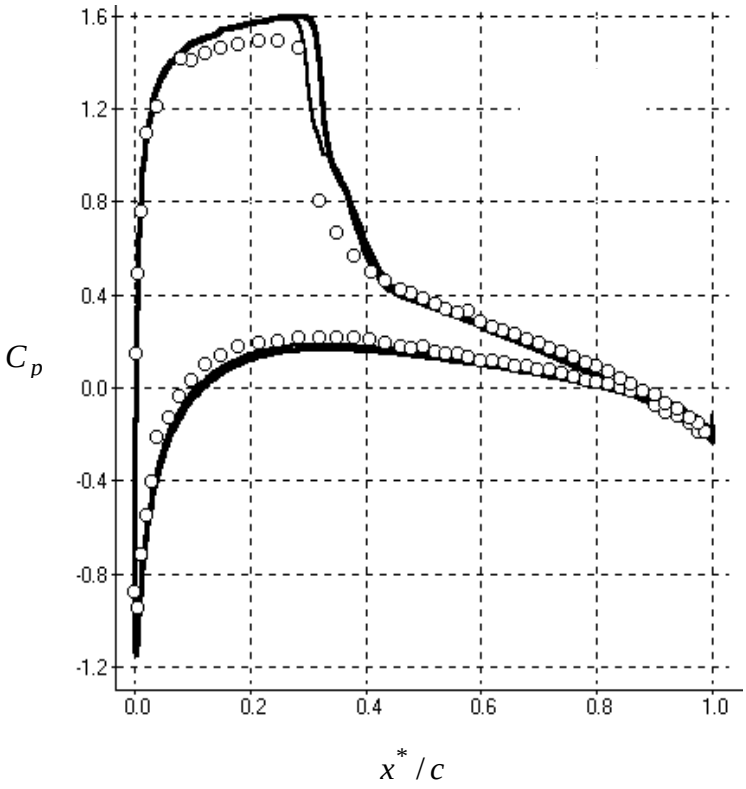


Fig. (15) The pressure coefficient distribution for the NACA 0012 transonic airfoil [8]

Where $C_p$ is the aerodynamic pressure coefficient, "$x^*$" is the coordinate along the wing chord and the "c" is the local cord length.

The pressure coefficient can be calculated using following equation

$$C_p = \frac{P - P_\infty}{q_\infty} \tag{8}$$

Where '$P$' is the local static pressure; $P_\infty$ is the free stream pressure and $q_\infty$ is the dynamic pressure.

For sure this pressure variation along the chord length results also in a variation in the lift force distribution along the chord, which by its role changes the

resulting shear forces and bending moments acting on the rib cross-section as shown in figure (16).

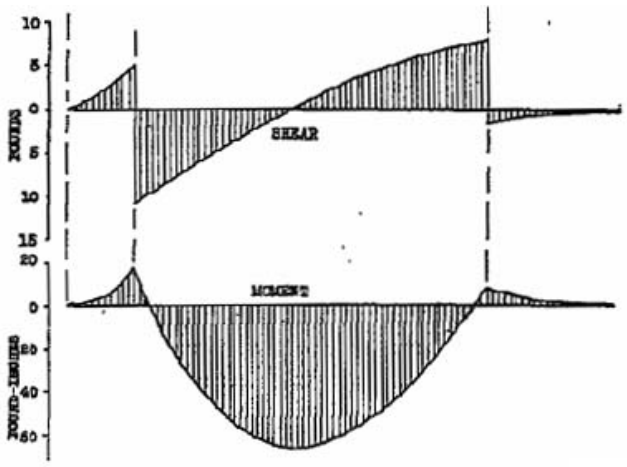


Fig. (16) General representation of the shear force and bending moment distribution acting on a wing rib [4].

But as an approximation, the resultant lift forces acting on certain cross-section along the wing span will be considered as concentrated force acting at the quarter chord length.

The loads calculated in Figures (13) and (14) are still not the actual DESIGN loads. They need to be scaled up by applying suitable scaling factors as these loads are too small to use for sizing the wing rib. The conditions of Mach = 0.75; CL=0.5 and *Re* = 0.3E7 is a cruise condition. Hence, a design condition of 2.5g maneuver is considered here and the obtained loads are multiplied by a factor 2.5 to make them the actual DESIGN loads. Also an additional safety factor of 1.5 is applied over these loads.

All these external aerodynamic loads will be resisted by internal reactions in the wing structure. The design of the stiffened panels is based on the assumption that the stringers are the members which are responsible about the bending resistance, while the skin is designed to just carry in plane stresses in the form of in plane shear stresses and tensile stresses, but its resistance to compressive stresses is very limited due to its instability under slightly compressive loads. The variation of the bending stress along the stiffened panels will generate a flexural shear flow in the plane of the airfoil.

## ***Calculation of Shear Flow:***

Unsymmetrical beam sections are very common in aircraft structure, because the airfoil shape is generally unsymmetric.

Considering a transversal load 'P' acting on an usymmetric cross-section passing through its shear center (i.e. the section is free of twisting), as shown in Figure (17)

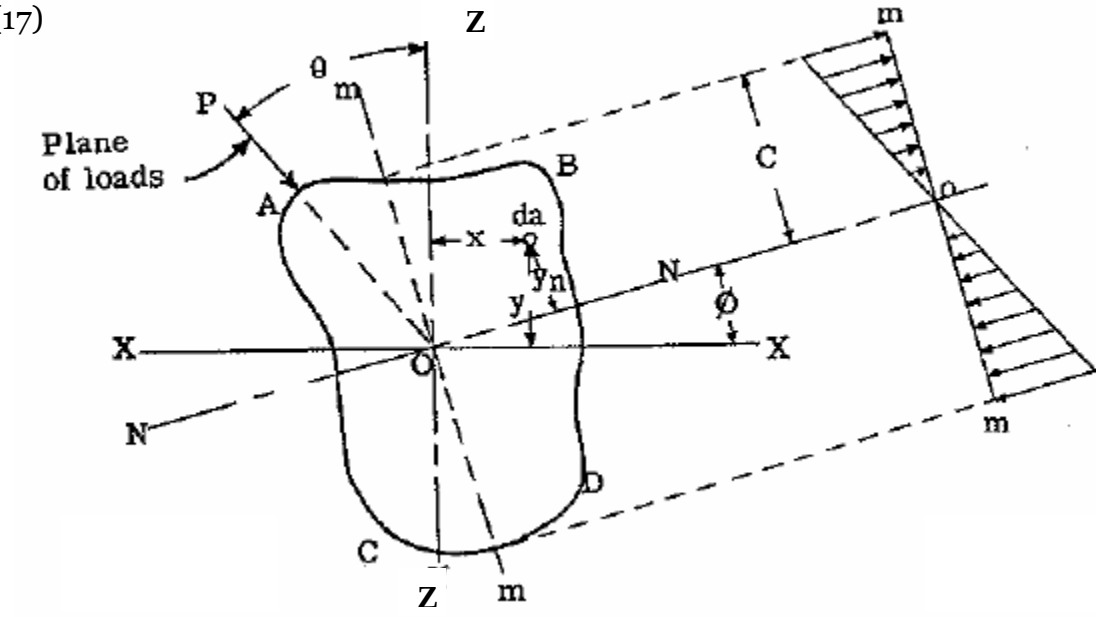


Fig. (17) Unsymmetrical cross-section of a straight cantilever beam [3]

Since this is an unsymmetrical cross-section beam, it is expected that its cross-section will warp under the effect of bending shear stresses, according to Saint-Venant's theory, but for simplification it is assumed here that the section is restrained of warping. Recalling from report (4), the equation of the bending stress in beams with unsymmetrical cross-sections, based on simple beam theory,

$$\sigma_b = -\frac{(M_x I_z - M_z I_{xz})}{I_x I_z - I_{xz}^2} z - \frac{(M_z I_x - M_x I_{xz})}{I_x I_z - I_{xz}^2} x \qquad (10)$$

Based on this equation, there are four methods, so far, for the derivation of the shear flow equations in beams with unsymmetrical cross-sections subjected to flexural shear stress namely, the principle axes method, the neutral axis method, the K-Method and the ($\Delta P$)-Method. The first three methods are dedicated for

beams with unsymmetrical but constant cross-sections along its span, i.e. its inertia moments are constant along the span while the fourth one is dedicated for beams with unsymmetrical and inconstant cross-sections (tapered sections). Following is a brief definition of each method.

## ***Method One: The Principle Axis Method***

This method is used for the calculation of the shear flow in beams with unsymmetrical but constant cross-sections. It is based on the calculation of the shear flow due to principle stresses. It is known that the product area moment of inertia '$I_{xz}$' is zero with respect to the principle axes, then equation (10) becomes

$$\sigma_b = -\frac{M_{xp} z_p}{I_{xp}} - \frac{M_{zp} x_p}{I_{zp}} \tag{11}$$

From this equation, the equation of the shear stress acting on the cross-section will be

$$\tau_b = -\frac{V_{zp}}{I_{xp} t}\int z_p dA - \frac{V_{xp}}{I_{zp} t}\int x_p dA \tag{11-a}$$

Where $\int z_p A$ and $\int x_p A$ are the first moments of area with respect to the X-X and Z-Z axes respectively and 't' is the thickness of the beam. These area moments of inertia can be calculated by superposition in case of composite cross-section areas.

From equation (11-a) the shear flow in the cross-section can be expressed as

$$q_b = -\frac{V_{zp}}{I_{xp}}\sum z_p A - \frac{V_{xp}}{I_{zp}}\sum x_p A \tag{11-b}$$

## ***Method Two: The Neutral Axis Method***

This method is used for the calculation of the shear flow in beams with unsymmetrical but constant cross-sections. It is based on the calculation of the shear flow due to stresses about the neutral axis of the cross-section N-N. Simply,

by resolving the stress obtained in method one into the neutral axis direction, the equation of the bending stress becomes

$$\sigma_b = \frac{M_n z_n}{I_n} \tag{12}$$

Where $I_n = I_{xp}\cos^2(a) + I_{zp}\sin^2(a)$, $z_n = z\cos(\phi) - x\sin(\phi)$ and $\tan(a) = -\frac{I_{xp}}{I_{zp}}\tan(\theta)$ where '$\theta$' is the angle formed between the transversal load and the '$Z$' axis while 'a' is the angle formed between the neutral axis and the 'X-X' axis, as shown in Figure (16).

From equation (12), the equation of the shear flow can be written as

$$q_n = \frac{V_n}{I_n}\sum z_n A \tag{12-b}$$

Where '$V_n$' is the shear force in the N-N direction.

## ***Method Three: The K-Method:***

This is the most widely used method for the calculation of the shear flow in beams with unsymmetrical and constant cross-sections. It is directly based on equation (10). From equation (10), it is possible to derive the equation of the flexural shear flow in the form

$$q = -(K_3 V_x - K_1 V_z)\sum xA - (K_2 V_z - K_1 V_x)\sum zA \tag{13}$$

Where $K_1 = \frac{I_{xz}}{I_x I_z - I_{xz}^2}$, $K_2 = \frac{I_z}{I_x I_z - I_{xz}^2}$, $K_3 = \frac{I_x}{I_x I_z - I_{xz}^2}$

## ***Method Four: The ($\Delta P$)-Method (for tapered sections):***

In airplane wing and fuselage structures, the common case is a beam of non-uniform section in the flange (stringer) direction. Figure (17-a) shows a single cell distributed flange beam. Consider the beam acts as a cantilever beam

with the bending moment existing at section (A) being greater than that existing at section (B) and that the bending moment produces compression on the upper surfaces. Using equation (10), the bending stress on each stringer can be found, which if multiplied by the stringer area gives the stringer axial load, as shown in the figure. Imagine the upper sheet panel 2-2$'$, 3-3$'$ is cut along the line (a-a). Furthermore consider stringer number (3) cut out and shown as a free body in Figure (17-b).

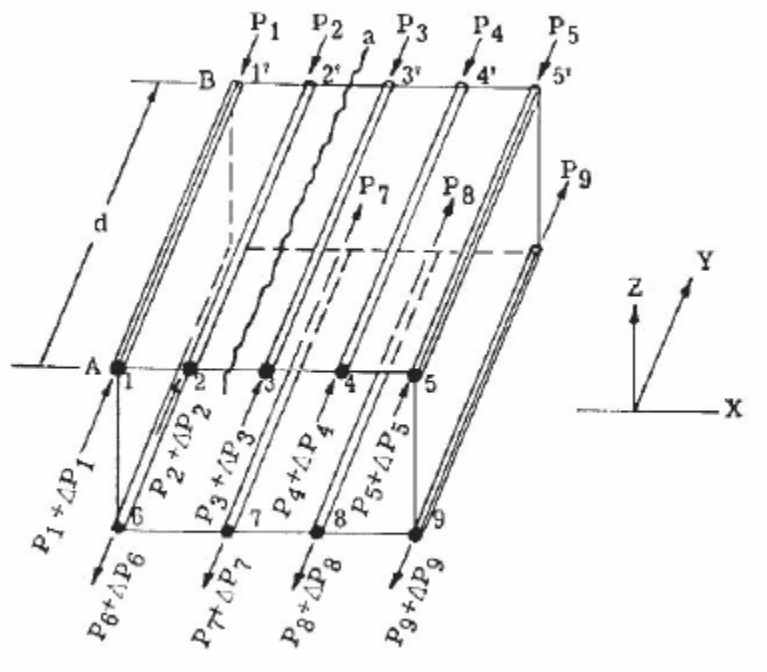


Fig. (17-a) Non-uniform beam cross section [3]

Let $q_y$ be the average shear flow per inch over the distance d on the sheet edge bb. For equilibrium of this free body, $\sum F_y = 0$, hence $\Delta p_3 + q_y d = 0$ then,

$$q_y = -\Delta p_3 / d \qquad (14)$$

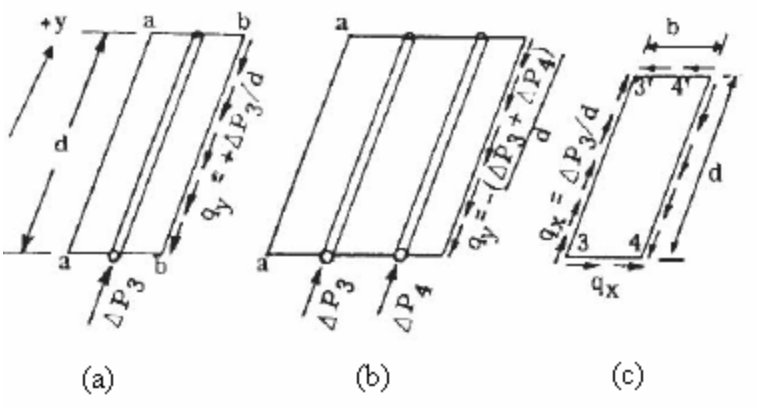


Fig. (17-b) Free body diagram of panels [3]

Figure (17-b-b) shows a free body diagram including two stringers or flange members. Again writing equilibrium in y direction gives $q_y = -(\Delta p_3 + \Delta p_4)/d$

Therefore starting at any place where the value of $q_y$ is known, the change in the average shear flow to some other section equals,

$$q_y = -\sum \frac{\Delta p}{d} \tag{14-a}$$

If the summation is started where $q_y$ is zero then equation (14-a) will give the true average shear flow $q_y$. Then the shear flow in the section at point 'n' can be represented generally as

$$q_{y_n} = q_o - \sum_{i=1}^{n} \frac{\Delta p_i}{d} \tag{15}$$

Figure (17-b-c) shows sheet panel (3, 3', 4, 4') isolated as a free body. Taking moments about corner 4' and equating to zero for equilibrium, gives $\sum M_{4'} = \frac{d(\Delta p_3)b}{d} - q_x bd$ where $q_x = \Delta p_3 / d$. Thus for rectangular sheet panels between flange members the shear flow $q_x$ or $q_z$ equals the average shear $q_y$.

Consider an element of the wing of length ‘dy’ extending from station ‘j’, located at an arbitrary station ‘$\eta_j$’ along the wing span, to station ‘j+1’.

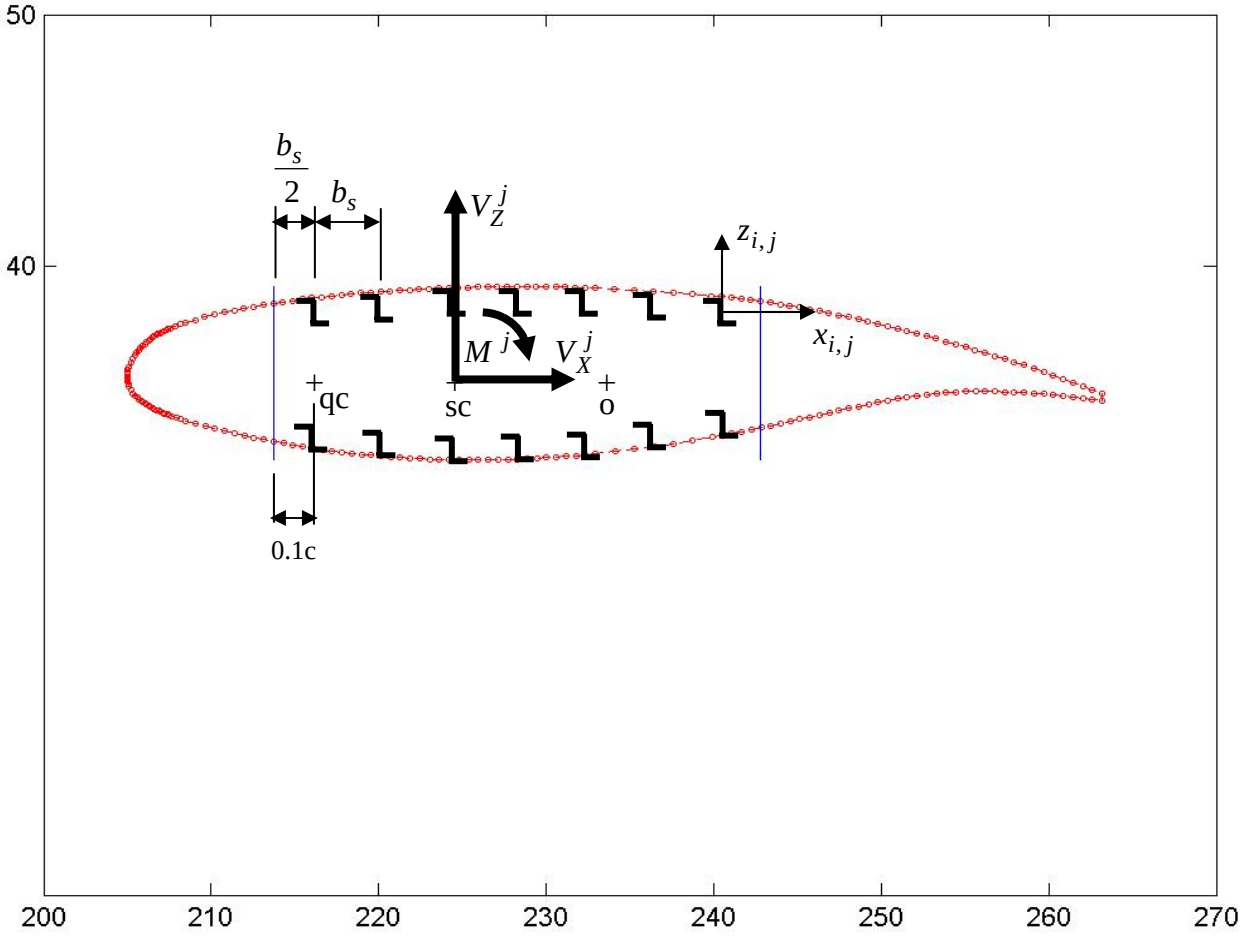


Fig. (18-a) Airfoil cross-section at an arbitrary ‘$\eta$’ along the wing span (Station-j)

Note that the superscripts in load notation belong to the station while the subscript belongs to the direction of that load.

Viewing this element in the spanwise direction shows the airfoil cross-section with the distribution of ‘Z’ stingers on the upper and lower skins at an arbitrary wing station $\eta$.

The side view of this element (either in the X-Y plane or Z-Y plane) can be seen as a tapered beam extending from station ‘j’ to station ‘j+1’, as shown in the following figure (for the Z-Y projection and by analogy the X-Y can be deduced)

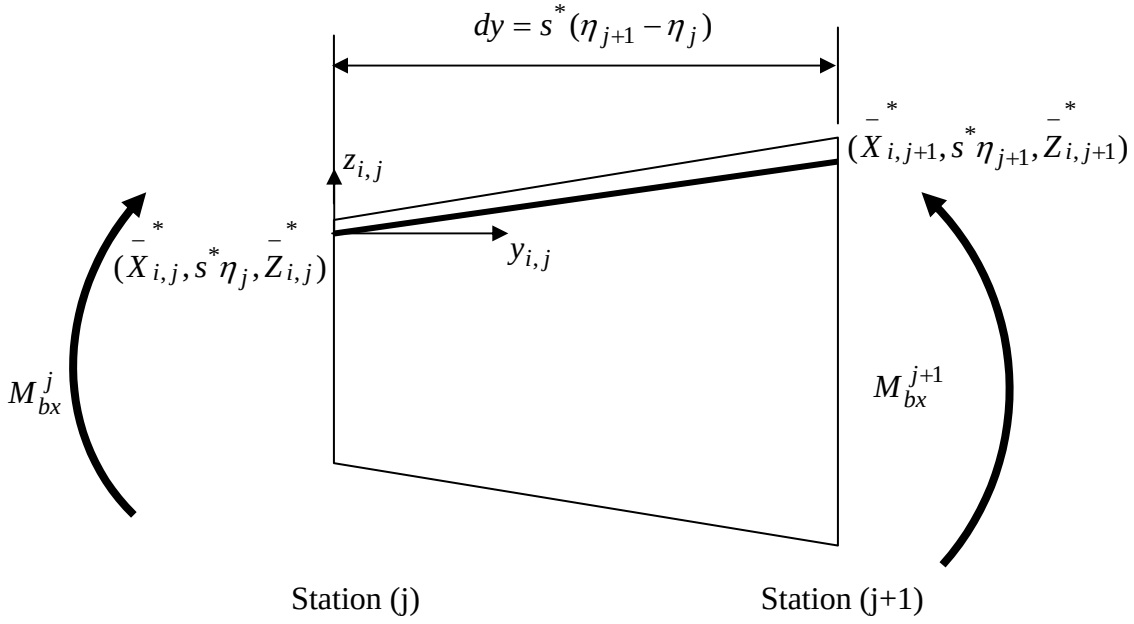


Fig. (18-b) side view of the wing element 'dy' extending from station 'j' to station (j+1) along the wing span

In figure (18-a), three main points are defined

- The quarter chord point (qc).

  This point is located at distance $\frac{c}{4}$ measured from the leading edge in the horizontal direction, where 'c' is the local chord length at that wing station. Since the front spar is located at 0.15c measured from the leading edge, then the quarter chord is located at distance 0.1c relative to the front spar.
- The centroid of the airfoil cross-section (o)
- The shear center of the airfoil cross-section (sc)

Also there is a local coordinate system $(x_{i,j}, y_{i,j}, z_{i,j})$ with its origin $(\bar{X}^*_{i,j}, s^*\eta_j, \bar{Z}^*_{i,j})$ located at the centroid of an arbitrary 'Z' stringer (*i*) in station (j) where this origin is defined with respect to the wing coordinate system, as shown in the figure.

The section is subjected to general arbitrary loading that are located at the shear center, as shown in the figure

- Two shear forces: a vertical shear force '$V_Z^j$' and a horizontal shear force '$V_X^j$'.
- Twisting moment '$M^j$'.
- Bending moment '$M_{bx}^j$' and $M_{bz}^j$.

## ***Calculation of section centroid:***

Since the stringers are assumed to carry the bulk of bending in skin-stringer sections, only the areas of the stiffeners are used in calculating the section centroid.

Recalling from the first report the details concerning the 'Z' stringer

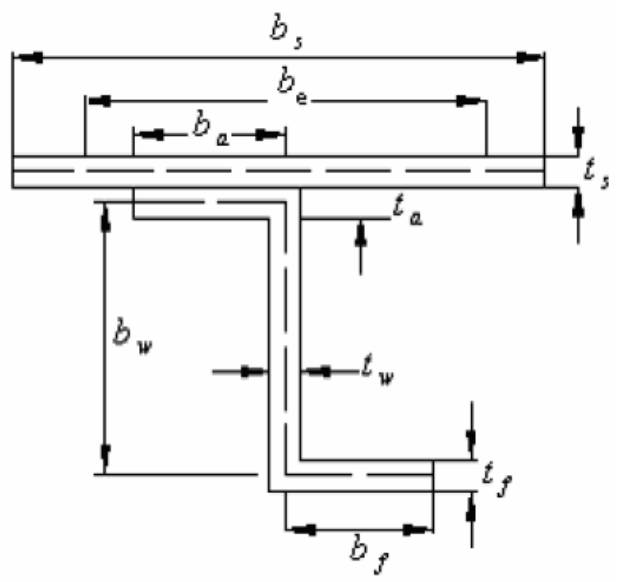


Fig. (19) Panel geometry definition using 'Z' stringer [5]

Where

$$b_a = 2.08t_s + 068 \quad if \quad t_s < 0.3 \quad and \quad b_a = 1.312 \quad if \quad t_s > 0.3$$

$$t_a = 0.7t_s$$

$$for\ equal\ flange\ atringers \qquad (16)$$

$$b_f = b_a \quad and \quad t_F = t_a$$

$$b_w = \sqrt{\left(\frac{b_e}{t_s}\right)\left(A_{st} - 1.4b_a t_a\right)}$$

'$A_{st}$' is the stringer cross-section area, and it can be represented as

$$A_{st} = (b_w - t_f)t_w + 2\left(b_f + \frac{t_w}{2}\right)t_f \tag{17}$$

And '$b_e$' is the effective width of the skin [5], where,

$$b_e = t_s\sqrt{K\frac{\eta E_{sk}}{\sigma_{sk}}} \tag{18}$$

where 'K' is the skin buckling coefficient and it takes the values

$$K = 3.62 \quad for \quad \frac{b_s}{t_s} < 40 \quad or \quad K = 6.32 \quad for \quad \frac{b_s}{t_s} > 110$$

Between the above values there is a gradual transition, as plotted in this figure

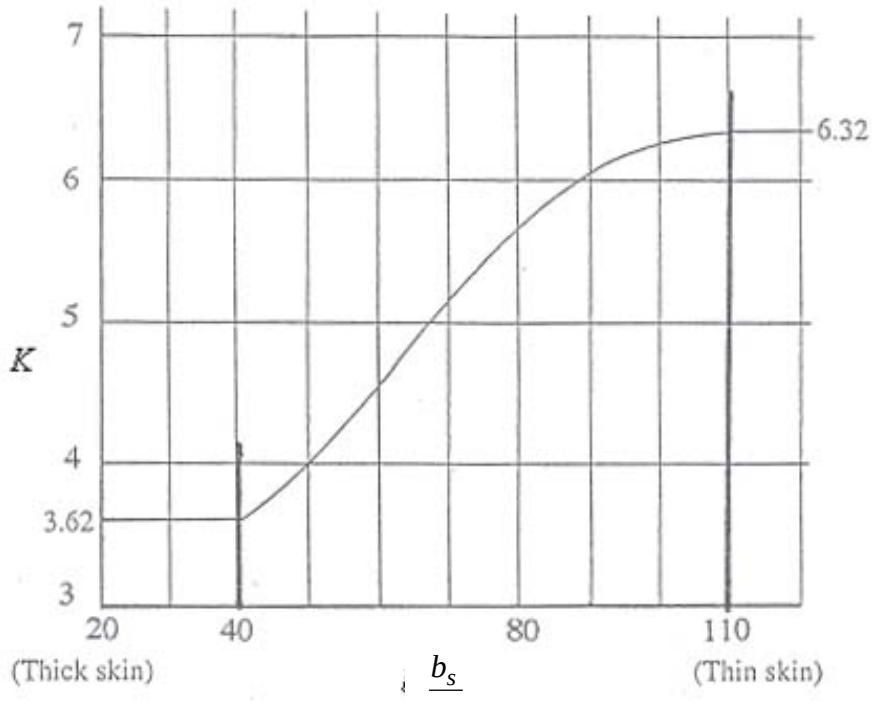


Fig. (19) Variation of compression panel skin buckling constant with skin cross-section aspect ratio [12]

'$\eta$' in equation (18) is the plasticity reduction factor which is determined using the following equation

$$\eta = \sqrt{\frac{E_{t\,sk}}{E_{sk}}} \tag{19}$$

Where '$E_{sk}$' and '$E_{t\,sk}$' are the elastic and tangent modulii of the skin, respectively While '$\sigma_{sk}$' is the skin axial stress.

For practical use, the design curves for the skin stringer panels can be used, where

$$\begin{aligned} &\frac{b_s}{b_e} = 1 && \text{for high value of load index } \frac{N}{L} \\ &\frac{b_s}{b_e} = 1.1:1.3 && \text{for low values of load index } \frac{N}{L} \end{aligned} \tag{20}$$

Where 'N' is the axial load intensity, and it can be calculated using the equation

$$N = \frac{M_b}{c_s h_s} \tag{21}$$

And 'L' is the effective column length, or the distance between two successive ribs.

All the coordinates defined in the previous figure is in the wing coordinate system $(x^*, y^*, z^*)$.

Using equation (17) the cross-section area of the i[th] stringer can be calculated as

$$A_{st\,i,j} = \left(b_{w_{i,j}} - t_{f\,i,j}\right) t_{w\,i,j} + 2\left(b_{f_{i,j}} + \frac{t_{w_{i,j}}}{2}\right) t_{f\,i,j} \tag{22}$$

Since it is assumed that the load variation along the wing chord will be considered constant (i.e. the dimensions of the stringers at certain wing station will be constant) then the subscript '*i*' in the previous equation can be eliminated.

For an airfoil cross-section with n-stringers, the centroidal coordinates will be

$$\begin{aligned} \bar{X}^*_j &= \frac{\sum_{i=1}^{n} A_{st_{i,j}}\, \bar{X}^*_{i,j}}{\sum_{i=1}^{n} A_{st_{i,j}}} \\ \bar{Z}^*_j &= \frac{\sum_{i=1}^{n} A_{st_{i,j}}\, \bar{Z}^*_{i,j}}{\sum_{i=1}^{n} A_{st_{i,j}}} \end{aligned} \tag{23}$$

Where $\bar{X}^*_{i,j}$ and $\bar{Z}^*_{i,j}$ are the coordinates of of the i[th] stringer cross-section centroid at the j[th] wing station with respect to the wing coordinate system $(x^*, y^*, z^*)$. While $\bar{X}^*_j$ and $\bar{Z}^*_j$ are the coordinates of the wing-box section centroid with respect to the wing coordinate system.

## ***Calculation of section moments of inertia:***

The inertia moment of the total section can be calculated, where

$$
\begin{aligned}
I_{\bar{X}_j} &= \sum_{i=1}^{n}\left( I_{\bar{X}_{i,j}} + A_{st_{i,j}}\left(\bar{Z}^*_{i,j} - \bar{Z}^*_j\right)^2\right) \\
I_{\bar{Z}_j} &= \sum_{i=1}^{n}\left( I_{\bar{Z}_{i,j}} + A_{st_{i,j}}\left(\bar{X}^*_{i,j} - \bar{X}^*_j\right)^2\right) \\
I_{\bar{X}_j \bar{Z}_j} &= \sum_{i=1}^{n}\left( A_{st_{i,j}}\left(\bar{Z}^*_{i,j} - \bar{Z}^*_j\right)\left(\bar{X}^*_{i,j} - \bar{X}^*_j\right)\right)
\end{aligned}
\qquad (24)
$$

Where $I_{\bar{X}_{i,j}}$ and $I_{\bar{Z}_{i,j}}$ are the local area moment of inertia of the i[th] stringer in the j[th] station, with respect to its local centroidal axes. For 'Z' stringers, the expressions for $I_{\bar{X}_{i,j}}$ and $I_{\bar{Z}_{i,j}}$ are

$$
\begin{aligned}
I_{\bar{X}_{i,j}} &= \frac{1}{6}\left(b_{a_j} + \frac{t_{w_j}}{2}\right)t_{a_j}^3 + \frac{1}{2}\left(b_{a_j} + \frac{t_{w_j}}{2}\right)t_{a_j} b_{w_j}^2 + \frac{1}{12}t_{w_j}\left(b_{w_j} - t_{f_j}\right)^3 \\
I_{\bar{Z}_{i,j}} &= \frac{1}{6}t_{a_j}\left(b_{a_j} + \frac{t_{w_j}}{2}\right)^3 + 2t_{a_j}\left(b_{a_j} + \frac{t_{w_j}}{2}\right)\left(\frac{b_{a_j}}{2} - \frac{t_{w_j}}{4}\right)^2 + \frac{1}{12}\left(b_{w_j} - t_{f_j}\right)t_{w_j}^3
\end{aligned}
\qquad (25)
$$

It is noted that the local product moment of inertia is zero, since the 'Z' stinger has centroidal axes of symmetry.

## ***Calculation of shear flow in the cross-section due to the shear forces*** $V_X^j$ ***and*** $V_Z^j$

As mentioned before there are different method for the calculation of the shear flow in unsymmetrical sections. The K-method is widely used but it is not strictly accurate in beams with tapered shape along the wing span. But it gives results with an acceptable approximation. For tapered sections which is a common case in aircraft structure the $(\Delta P)$ method is much more accurate than the K-method since it considers the variation of the elastic properties of the structural sections in the calculation. Following is a brief description of using the two methods in calculating the shear flow in the section shown in figure (18-a).

## ***The K-Method***

Substitute the inertia moments obtained in equation (24) into equation (13)

$$q'_j = -(K_3 V_X^j - K_1 V_Z^j)\sum\left(\bar{X}^*_{i,j} - \bar{X}^*_j\right)A_{st_j} - (K_2 V_Z^j - K_1 V_X^j)\sum\left(\bar{Z}^*_{i,j} - \bar{Z}^*_j\right)A_{st_j} \qquad (26)$$

This equation gives the general formula for the shear flow in the wing box j[th] station Where $K_1 = \dfrac{I_{\bar{X}_j \bar{Z}_j}}{I_{\bar{X}_j} I_{\bar{Z}_j} - I^2_{\bar{X}_j \bar{Z}_j}}$, $K_2 = \dfrac{I_{\bar{Z}_j}}{I_{\bar{X}_j} I_{\bar{Z}_j} - I^2_{\bar{X}_j \bar{Z}_j}}$, $K_3 = \dfrac{I_{\bar{X}_j}}{I_{\bar{X}_j} I_{\bar{Z}_j} - I^2_{\bar{X}_j \bar{Z}_j}}$

The calculation of the shear flow with respect to an external shearing force requires starting the calculation from a point where the shear flow is known. Accordingly, assume that the skin between stinger (*i-1*) and stinger (*i*) is cut. This way the shear flow in the skin extending between those two stingers becomes zero. Then the shear flow in the skin extending between stringer (*i*) to stringer (*i+1*) can be expressed as

$$\left(q'_{i\to i+1}\right)_j = \left(q'_{i-1\to i}\right)_j +$$

$$\left[-(K_3 V_X^j - K_1 V_Z^j)\sum\left(\bar{X}^*_{i,j} - \bar{X}^*_j\right)A_{st_j} - (K_2 V_Z^j - K_1 V_X^j)\sum\left(\bar{Z}^*_{i,j} - \bar{Z}^*_j\right)A_{st_j}\right] \qquad (26\text{-a})$$

After calculating the shear flow around the cross-section, return the skin previously removed between stingers (*i-1*) and stinger (*i*), then the present value of the shear flow is not the actual value. Since the previous shear flow is calculated for an open cross-section, which is not the case. Accordingly, a further analysis is needed to calculate the actual value of the shear flow for a closed section.

The twisting angle of a section can be expressed as

$$\theta_j = \frac{1}{2A_{sj}G}\sum_{i=1}^{n-1}\frac{\left(q_{i\to i+1}\right)_j\left(s_{i\to i+1}\right)_j}{\left(t_{i\to i+1}\right)_j} \tag{27}$$

Where '$A_{sj}$' is the area of the wing-box cross section at the '$j^{th}$' station, '$\left(s_{i\to i+1}\right)_j$' is the distance between stringer (*i*) and stringer (*i+1*), 'G' is the shear modulus of the skin material and '$\left(t_{i\to i+1}\right)_j$' is the skin thickness between stringer (*i*) and stringer (*i+1*) in the $j^{th}$ station.

Since the shear forces are passing through the shear center which implies that the section is not subjected to any kind of twist due to these shear forces (i.e. the section twisting angle is equal to zero).

Now, assume that there is a constant shear flow '$q_0$' acting around the cross-section in the positive clockwise direction, in addition to the shear flow calculated previously for the open section. Substituting in equation (27) and equate it to zero, the value of '$q_{0,j}$' can be obtained. Then the actual shear flow around the cross-section between the '*i*' and the '*i+1*' stringers is equal to

$$\left(q_{i\to i+1}\right)_j = \left(q'_{i\to i+1}\right)_j + q_{0,j} \tag{27-a}$$

If the shear center coordinates are already calculated then the secondary shear flow '$q_{0,j}$', calculated in the previous step, can also be calculated by considering the moment equilibrium of the internal loads represented by the shear flow '$q'$' in addition to the constant shear flow '$q_0$' around the whole section, with the external loads acting on the cross-section. Since all the external loads, $V_Z^j$ and $V_X^j$ are passing through the section shear center, then considering moment

equilibrium with respect to the shear center will eliminate the moment component of these external forces. While the moment of the shear flow with respect to the shear center can be calculated using the equation

$$\sum M\big|_{q_j^{'}} + 2A_{sj}q_{0,j} = 0 \qquad (28)$$

Where '$A_{sj}$' is the area of the wing-box cross section at the '$j^{th}$' station while $\sum M\big|_{q_j^{'}}$ is the summation of the moments of the shear flow $q_j^{'}$ between two adjacent stringer, which can be calculated as

$$\sum M\big|_{q_j^{'}} = 2\sum \left(A_{i,i+1}\right)_j \left(q^{'}{}_{i\to i+1}\right)_j \qquad (28\text{-a})$$

Where $\left(A_{i,i+1}\right)_j$ is the area enclosed between the skin between stingers '$i$' and '$i+1$' and the two lines extending from each stringer to the shear center of the cross-section.

It is advantageously to note that, if the external twisting moment '$M^j$' acting on the cross-section, shown in figure (18-a), is included in equation (29) of moment equilibrium, then the global shear flow around the section can be calculated. Then equation (29) can be written as

$$\sum M\big|_{q_j^{'}} + M^j + 2A_{sj}q_{0,j} = 0 \qquad (28\text{-b})$$

## ***The ($\Delta P$)-Method***

This method is accurate for shear flow calculations in tapered sections which is the case presented here.

In this method the axial forces in stringers at two wing stations should be calculated. Considering stations (j) and (j+1), the axial forces in the stingers at the two stations can be obtained by calculating the bending moment in each stringer at each station, then multiplying the bending moment by the area of each stringer gives the axial force in the stinger.

Recalling equation (10), the bending moment in the $i^{th}$ stringer in the $j^{th}$ station can be calculated as

$$\sigma_b^{i,j} = -\frac{(M_{bx}^{j} I_{\bar{Z}_j} - M_z I_{\bar{X}_j \bar{Z}_j})}{I_{\bar{X}_j} I_{\bar{Z}_j} - \left(I_{\bar{X}_j \bar{Z}_j}\right)^2}\left(\bar{Z}^{*}_{i,j} - \bar{Z}^{*}_{j}\right) - \frac{(M_{bz}^{j} I_{\bar{X}_j} - M_{bx}^{j} I_{\bar{X}_j \bar{Z}_j})}{I_{\bar{X}_j} I_{\bar{Z}_j} - \left(I_{\bar{X}_j \bar{Z}_j}\right)^2}\left(\bar{X}^{*}_{i,j} - \bar{X}^{*}_{j}\right) \tag{29}$$

Then, the axial force acting on the i$^{th}$ at that wing station is

$$P_{i,j} = \sigma_b^{i,j} A_{st_{i,j}} \tag{29-a}$$

By the same manner the axial force in the i$^{th}$ stringer in the 'j+1' station can be represented as

$$P_{i,j+1} = \sigma_b^{i,j+1} A_{st_{i,j+1}} \tag{29-b}$$

Then the variation in the axial force along the 'i$^{th}$' stinger along the stations 'j' and 'j+1' is

$$\Delta P_i = P_{j+1} - P_j \tag{30}$$

Substituting in equation (17-a), then the average shear flow '$q_{y_n}$' can be calculated as

$$q_{y_n} = q_o - \sum_{i=1}^{n} \frac{\Delta P_i}{s^{*}\left(\eta^{*}_{j+1} - \eta^{*}_{j}\right)} \tag{31}$$

Based on the equality of the shear flow in all directions at certain point inside continua, then the shear flow in the skin extending between stinger 'i' and stinger 'i+1' in the 'j' wing station will be

$$\left(q'_{i \to i+1}\right)_j = \left(q'_{i-1 \to i}\right)_j + \left(-\frac{\Delta P_i}{s^{*}\left(\eta^{*}_{j+1} - \eta^{*}_{j}\right)}\right) \tag{31-a}$$

It is clear that the calculation of the shear flow should begin at a point where the value of the shear flow is known. Accordingly, assume that the skin between the 'i-1' and the 'i' stingers is cut, that makes the value of $q'_{i-1 \to i}$ is equal to zero,

which enables the use of the previous equation. As mentioned before, these values of shear flow distribution obtained by the previous equation is not the actual value. To obtain the actual value, an additional constant shear '$q_o$' flow around the whole cross-section will be applied, where the total actual shear flow between adjacent stringers can be calculated as

$$\left(q'_{i\to i+1}\right)_j = q_o + \left( -\frac{\Delta P_i}{s^*\left(\eta^*_{j+1} - \eta^*_j\right)} \right) \qquad (31\text{-b})$$

While the value of '$q_o$' can be obtained as discussed in the K-method.

## ***Calculation of the shear center coordinates:***

The shear center is a geometrical property of the cross-section. It is the point on the cross-section that if a shear force is passing through will not twist the section. Accordingly, if there is a force acting on the cross-section that is not passing through its shear center, then the effect of that force on the cross-section can be split into two parts,

1) flexural shear effect due to the shear force
2) torsional shear effect due to the twisting effect of that force on the cross-section, this twisting moment takes the value of '*Ve*' where 'V' is the shear force and 'e' is the perpendicular distance between the cross-section shear center and the line of action of the shear force.

The shear center coordinates can be obtained with respect to any reference point on the cross-section. Since the section centroid is already defined, then the shear center can be calculated with respect to it

To calculate the shear center coordinates,

1) the horizontal location of the shear center '$e_{X_j}$':

   '$e_{X_j}$' is the horizontal distance between the cross-section centroid and its shear center. To find this distance:

a) Assume that there is only one vertical shear force '$V_Z^j$' acting on the cross-section passing through its shear center 'sc'.
b) Calculate the shear flow around the cross-section in terms of this shear force, as explained previously.
c) Calculate the moment of the external shear force '$V_Z^j$' with respect to the section centroid and equate it to the moment of the shear flow with respect to the same point.

$$\sum M\big|_{q_j} = V_Z^j e_{X,j} \tag{32}$$

Where $\sum M\big|_{q_j}$ is the moment of the shear flow with respect to the section centroid, which is computed using the equation (28-a).

2) the vertical location of the shear center '$e_{Z_j}$':

'$e_{Z_j}$' is the vertical distance between the cross-section centroid and its shear center. The same procedure can be used to find this distance, where:

a) Assume that there is only one horizontal shear force '$V_X^j$' acting on the cross-section passing through its centroid 'o'.
b) Calculate the shear flow around the cross-section in terms of this shear force, as explained previously.
c) Calculate the moment of all these shear forces with respect to the section centroid and equate it to the moment of the shear force with respect to the centroid.

$$\sum M\big|_{q_j} = V_Z^j e_{Z_j} \tag{33}$$

## ***Calculation of wing station external loads:***

As previously defined, the 'j$^{th}$' wing station is subjected to three type of loading

1. **Shear forces in the form of:**

   a. **Vertical shear force** $V_Z^j$

   This vertical shear force includes:

   (i) The total lift summation from the wing tip till the 'j$^{th}$' wing station which can be obtained from figure (13) for the DLF-6 aircraft. This value of shear force obtained from figure (13) must be multiplied by maneuvering condition factor plus safety factor for load and calculation tolerances.

   (ii) Wing structural weight (body forces) included in the wing portion extending from the wing tip till the 'j$^{th}$' station. It is important to note that in the conceptual design stage the size of the wing parts is not yet determined. Accordingly, the weight of the wing portions will not be available. Alternatively, an approximate value for the distribution of the wing weight along the wing span can be obtained from previously designed airplanes, or the weight may not be included in the initial sizing process, then it can be included later then an iteration design process can be conducted for a suitable convergence for the wing weight.

**Example on weight estimate**: the wing semi-span of the aircraft under consideration, DLR-F6, is '$s^* = 463.3 in.$', based on that data for an aircraft with approximately similar dimensions can be obtained. The Boeing 737-500 has a semi span length of 466.2 in. as shown in the next figure

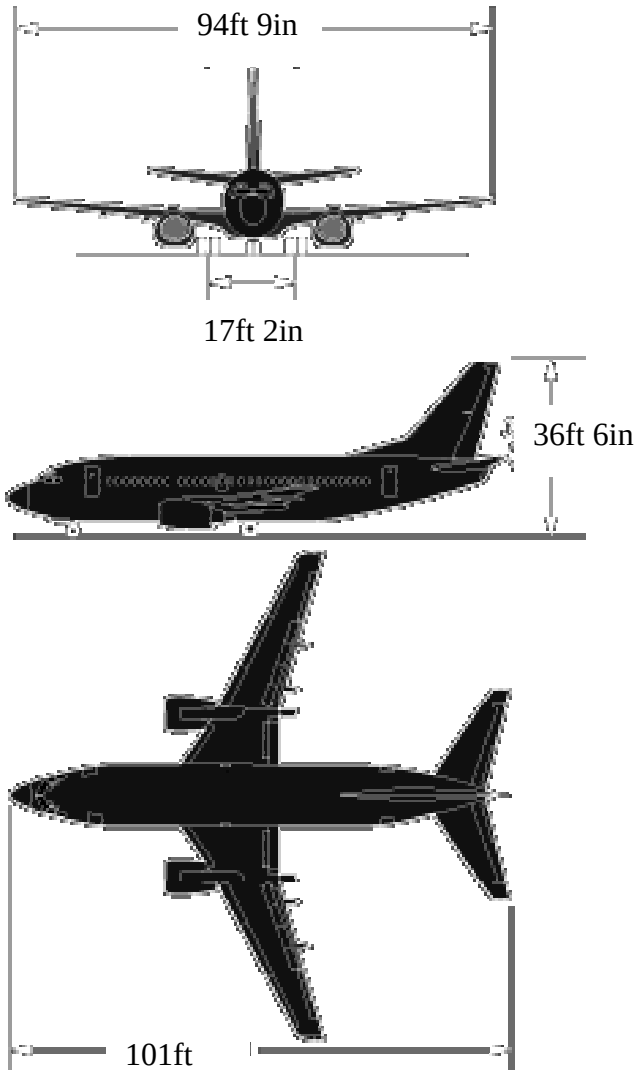


Boeing 737-500 main dimensions

Using weight statement of this aircraft, then the weight of the total wing system 12,255 lbs. using this weight with the length of the wing span, an approximate value for the wing weight, as a uniformly distributed load acting downwards along the wing span through acting along sections centroid, can be calculated and applied along the which in this case will be (12 lbs/in.).

(iii) Inertia forces (body forces), where the mass of the wing portion structure must be multiplied by the acceleration of flight in the vertical direction.

(iv) Non-structural mass forces due to the fuel tank weight…etc. in the form of weight and inertia forces.

**b. Horizontal shear force** $V_X^j$

This horizontal shear force includes:

(i) The total drag summation from the wing tip till the 'j$^{th}$' wing station. This value of the drag force obtained from wind tunnel calculations must be multiplied by maneuvering condition factor plus safety factor.

(ii) Inertia forces (body forces), where the mass of the wing portion structure must be multiplied by the acceleration of flight in the horizontal direction.

(iii) Non-structural mass forces due to the fuel tank mass…etc. in the form of inertia forces.

**2. Twisting moment**

As previously defined the wing station is subjected to twisting moment '$M^j$' the sources of this twisting moment are

(i) The pitching moment $M_{qc}^j$. The pitching moment about quarter chord location for DLR-F6 can be obtained from figure (12). It is important to note that the value of the pitching moment obtained from figure (12) must be multiplied by a factor of safety as well as a maneuvering conditions factor to obtain design loads.

(ii) Twisting effect of lift forces.

The lift force is always calculated with respect to the aerodynamic center of the wing cross-section which with an acceptable approximation considered as the airfoil quarter chord location. This lift force at the quarter chord has a twisting effect with the value of $V_Z^j e_{X_j}$.

(iii) Flange forces twisting moment '$M_f^j$':

As shown in figure (18-b), the aircraft has a tapered wing, which implies that the stiffeners are not perpendicular to the airfoil cross-

section but they have inclination angle in the Y-Z plane as well as in the Y-X planes. These inclinations generate a flange force components in the three space directions $F^{j}_{f_{X,i}}$, $F^{j}_{f_{Y,i}}$ and $F^{j}_{f_{Z,i}}$.

In the calculation of the shear flow around the airfoil cross-section the in-plane forces are of quite importance to the calculations. $F^{j}_{f_{X,i}}$ and $F^{j}_{f_{Z,i}}$ are the '$i^{th}$' stringer in the '$j^{th}$' wing station flange forces in the X and Z directions respectively. These forces are generating a flexural shear effect as well as a twisting effect on the airfoil cross-section.

(iv) Twisting effect of the drag forces:

the general shape of the airfoil is shown in figure (18-a) and the drag forces are always considered as acting horizontally through the quarter length of the airfoil chord line, as shown in the following figure

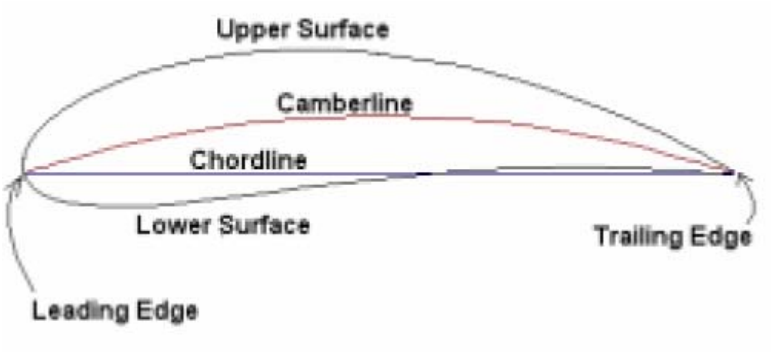


Fig. (20) Airfoil main lines

If the line of action of the drag forces is not passing with the airfoil shear center, then a twisting effect takes place with magnitude $V^{j}_{X} e_{Z_j}$.

(vi) Twisting effect wing portion weight:

Once the wing weight included in the design process, a twisting effect of the wing portion weight must be introduced, the magnitude of this twisting moment is '$W_j e_0$' where $W_j$ is the weight of the wing portion extending from the wing tip till wing station 'j' and $e_0$ is the horizontal

distance between the airfoil centroid and shear center at that wing station.

## ***II-3-2 Concentrated Loads:***

The design of the ribs is based on the assumption of the idealized beam, that the stiffeners are the responsible about carrying the entire axial load, while the shear webs are just loaded in pure shear. Accordingly, the arrangement of the stiffeners in the web differs according to the location and direction of the concentrated force acting on the rib. The following is a summary for different cases of concentrated loads and the corresponding stiffeners arrangements:

1) If the concentrated force is applied in the plane of the rib, then the stiffener should be aligned with the line of action of the force.
2) If placing the stiffener to be aligned with the load is impossible due to some openings in the rib, cutouts…etc, then placing two inclined stiffeners is also acceptable, since each stiffener will carry a component of the load in its direction.
3) If the load is out of plane of the rib, then placing three stiffeners perpendicular to each other is also acceptable since each stiffener will carry a component of the force in its direction, as shown in figure (21)

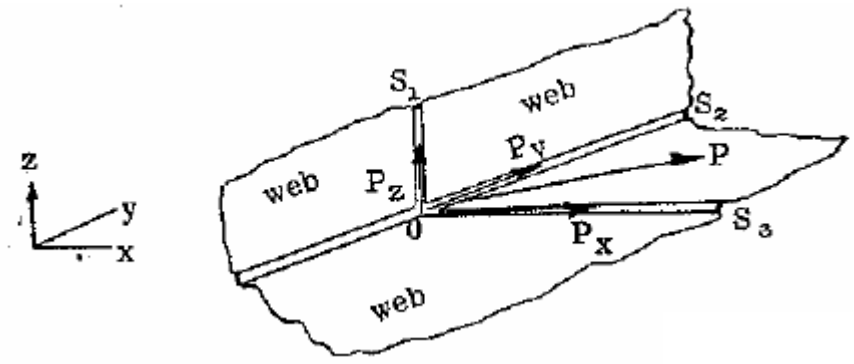


Fig. (21) the stiffeners arrangement in a shear web subjected to out-of-plane concentrated force [3]

4) If the load is normal to the web, then design of stronger flanges to carry the load in bending then transfer it to the web.

## ***Calculation of Shear Flow due to concentrated forces:***

In a similar manner as mentioned in the previous section, the concentrated load will be resolved in the 'x' and 'z' directions then it will be added to the shear force components mentioned previously.

## ***II-4 Shear Panel Stability:***

As mentioned before the design of the shear panels, like the wing rib panel, is based on the assumption of the idealized beam theory, that the panels are always loaded in pure shear.

Using Mohr circle, it is easy to conclude that if a point in a structure is subjected to pure shear, it will have two principle stresses at planes forming $45^{o}$ with the plane of the shear stress. One of these two principle stresses is in tension and the other one is in compression and the magnitude of the two stresses is equal to the magnitude of the shear stress, as shown in figure (22)

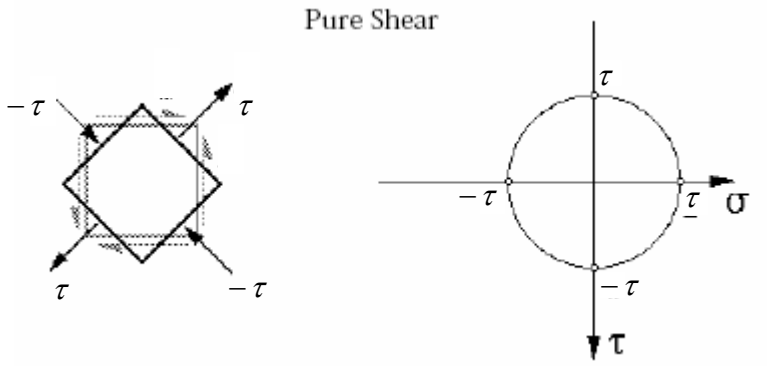


Fig. (22) Element of Structure subjected to pure shear [11]

So it is important to note that once the value of the compressive principle stress reaches certain critical value, the panel will buckle.

## ***II-4-1 Thin Plate Buckling:***

A thin plate is a flat sheet of material, the thickness of which is very much smaller than its lateral dimensions.

Figure (23) shows an 'a' by 'b' buckled rectangular plate of uniform thickness 't'. the middle surface of the plate, the surface lies in between the top and the bottom surfaces, is initially in the x-y plane. The opposite edges of the plate, the edges at 'x=0' and 'x=a' are simply supported while the other two edges are free. The simply supported edges are subjected to uniform compressive stress $\sigma_{cr}$ .

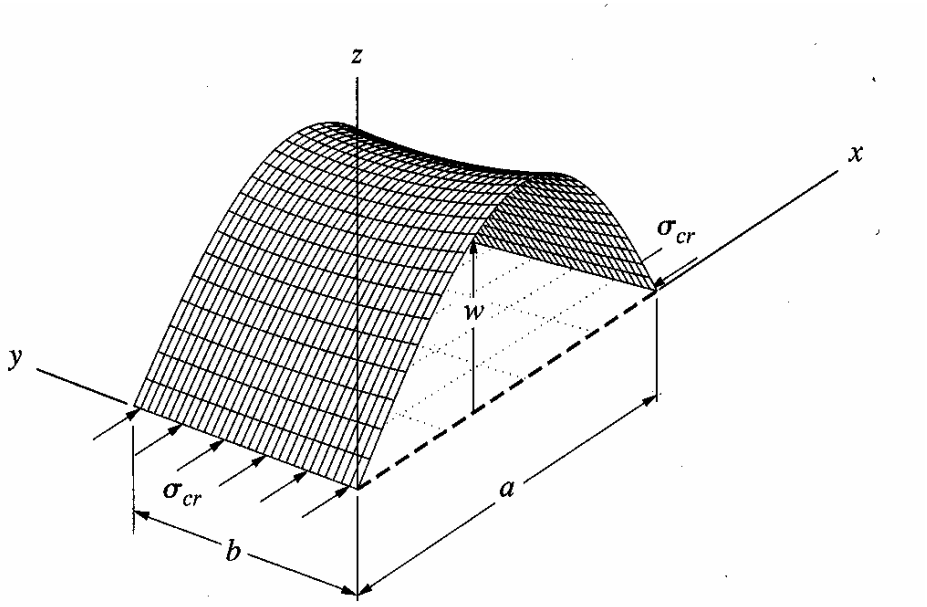


Fig. (23) Buckled shape of a plate buckled with unsuspended sides and loaded in compression on its simply-supported ends [11]

Thin plates are capable of supporting loads normal to its surface in addition to membrane forces that lie in the plane of the plate. But, compressive in-plane stresses cause the plate to buckle at stresses much lower than its yielding stress limit.

It is very important to determine the value of the stress at which the plate starts buckling, because the structure at that value is considered as an unstable structure and post buckling analysis should takes place because of the redistribution of stresses.

Since the magnitude of the compressive stress acting on the plate in Figure (22) is the critical buckling stress value, buckling will take place.

Viewing this plate in the x-z plane, it will look like a pined-pined column, as shown in figure (24).

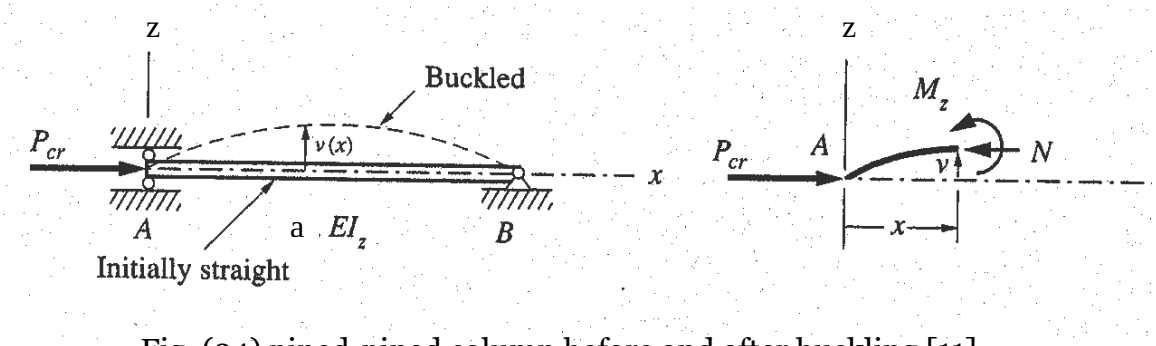


Fig. (24) pined-pined column before and after buckling [11]

After buckling, the column can be considered as a simple beam in bending, using simple beam theory, and neglecting the shear, the equation of motion of this column will be,

$$\frac{d^2\nu}{dx^2} + \frac{P_{cr}}{EI_z}\nu = 0 \tag{34}$$

Where '$\nu$' is the lateral displacement of the column in the x-z plane.

The solution of this homogenous differential equation is

$$\nu = A\sin\lambda x + B\cos\lambda x \tag{35}$$

Where $\lambda = \sqrt{\frac{P_{cr}}{EI_y}}$, while A and B are constants to be determined from boundary conditions.

Applying the boundary conditions, will lead to the results that

$$P_{cr} = n^2\frac{\pi^2 EI_y}{a^2} \tag{36}$$

Where 'n' is the buckling mode. Since we are interested in the first buckling mode, then $P_{cr} = \frac{\pi^2 EI_y}{a^2}$.

Applying this critical value of the buckling load into the plate in figure (23), then

$$\sigma_{cr} = \frac{P_{cr}}{A} = \frac{P_{cr}}{bt} = \frac{\pi^2 E t^2}{12a^2} \tag{37}$$

The use of equation (37) in the case of a plate is not strictly correct, because in the simple beam theory the Poisson's effect is neglected, which can not be neglected in the case of a plate. Therefore, equation (37) is modified to the following equation

$$\sigma_{cr} = C_1 \frac{\pi^2 E}{12(1-\nu^2)}\left(\frac{t}{a}\right)^2 \tag{38}$$

Where '$C_1$' is a factor depends on Poisson's ratio as well as the aspect ration of the plate 'a/b'. The variation of '$C_1$' with the aspect ratio for certain Poisson's ratio is shown in the following figure

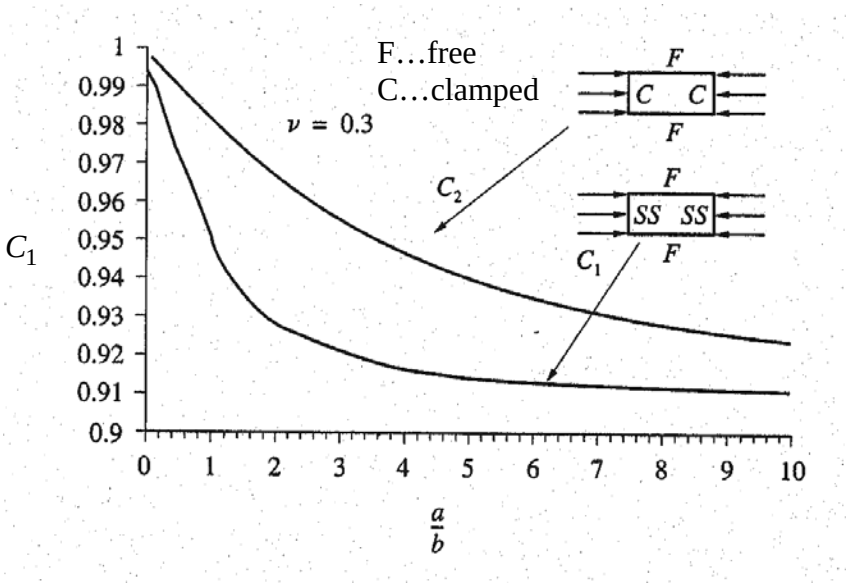


Fig. (25) Variation of '$C_1$' with the aspect ratio (Approximate) [11]

The exact derivation of the equation of the critical compressive stress is based on the solution of the plate differential equation of motion in buckling, which can be represented by the following equation

$$\frac{\partial^4 w}{\partial x^4} + 2\frac{\partial^4 w}{\partial x^2 \partial y^2} + \frac{\partial^4 w}{\partial y^4} = \frac{12(1-\nu^2)}{Et^4}\left(\sigma_x \frac{\partial^2 w}{\partial x^2} + \sigma_y \frac{\partial^2 w}{\partial y^2} + 2\tau_{xy}\frac{\partial^2 w}{\partial x \partial y}\right) \tag{39}$$

And the solution of this equation will lead to the formula of the critical buckling stress in rectangular plates

$$\sigma_{cr} = C\frac{\pi^2 E}{12(1-\nu^2)}\left(\frac{t}{b}\right)^2 \tag{40}$$

Where 'C' is a constant depends on the boundary conditions, Poisson's ratio and the aspect ratio of the rectangular plate, as shown in the next figure.

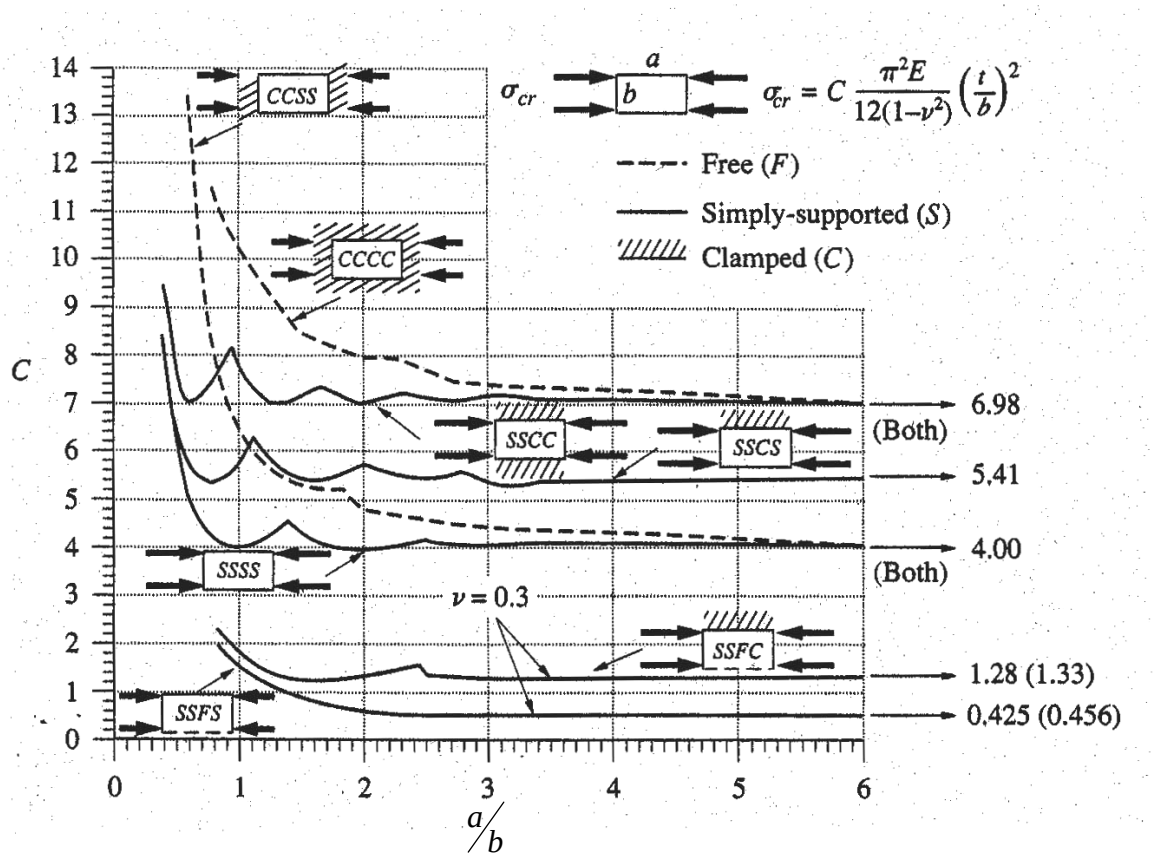


Fig. (26) Coefficient 'C' versus the aspect ratio for several boundary conditions (Based on Exact Formulation Exact) [11]

So it is important to note that once the value of the compressive principle stress in the shear panel reaches the value of '$\sigma_{cr}$' the panel will buckle. Accordingly, there is also a critical value for the shear stress, at which the panel will buckle

$$\tau_{cr} = C_s\frac{\pi^2 E}{12(1-\nu^2)}\left(\frac{t}{b}\right)^2 \tag{41}$$

'$C_s$' is a shear constant that depends on the aspect ratio of the plate, Poisson's ratio and the boundary conditions. If the buckling occurs at stress values higher than the proportional limit of the stress-strain relation, the previous equation should be modified to

$$\tau_{cr} = \eta_s C_s \frac{\pi^2 E}{12(1-\nu^2)}\left(\frac{t}{b}\right)^2 \tag{42}$$

Where '$\eta_s$' is called the plasticity correction factor, where

$$\eta_s = \frac{G_s}{G} \tag{43}$$

Where 'G' is the shear modulus and '$G_s$' is the shear secant modulus of elasticity which can be obtained from shear stress-strain diagram for the material.

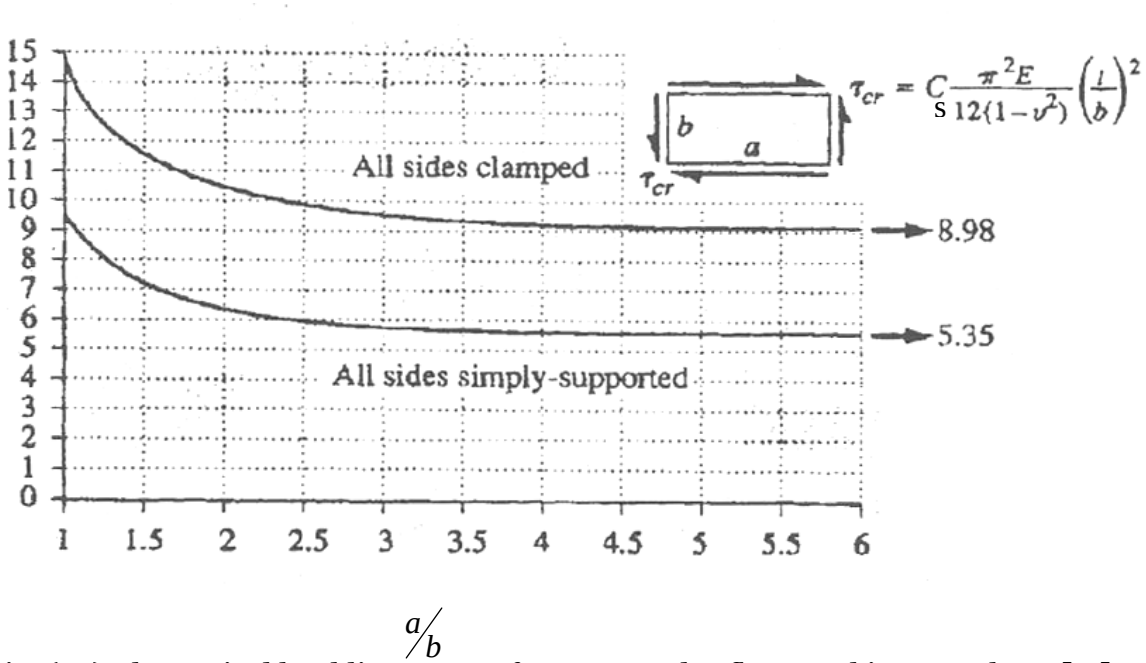


Fig. (27) Theoretical buckling curves for rectangular flat panel in pure shear [11]

Figure (27) shows the variation of shear buckling coefficient with the aspect ratio of a rectangular plate for different boundary conditions.

It is important to mention that the value of '$C_s$' shown in the previous curve is for flat panels.

For curved panels, the value of '$C_s$' changes dramatically with the value of the radius of curvature of the panel, as shown in the next figures

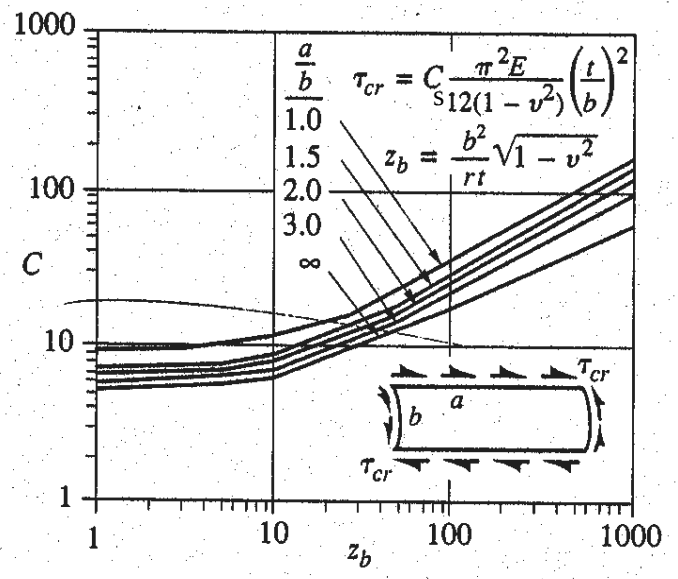


Fig.(28-a) Theoretical shear buckling coefficient for long, simply supported curved panels [11]

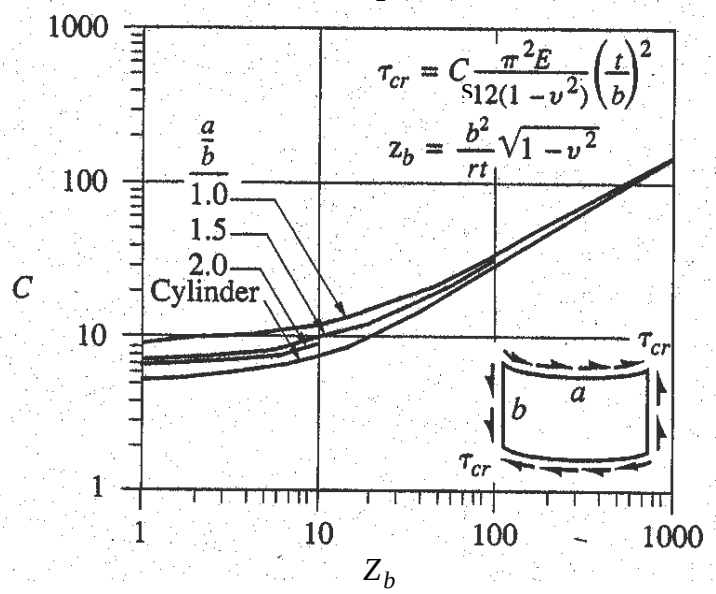


Fig. (28-b) Theoretical shear buckling coefficient for short simply supported curved panels [11]

Where $Z_b$ in the abscissa is represented by the equation

$$Z_b = \frac{b^2}{rt}\sqrt{1-\nu^2} \qquad (44)$$

This variable indicates the curvature of the panel.

Curved shells are sensitive to initial imperfections. Tests show that buckling may occur at stresses below those predicted by theory. Thus, the theoretical buckling curves are not strictly conservative, but they are useful in the conceptual design stage, where they can provide round figure for different dimensions. But, additional empirical information may be required to accurately predict the buckling strength.

## ***II-4-2 Diagonal Tension Field Beam:***

Once the value of this compressive stress reaches its critical value, the web buckles forming what is called diagonal tension field state. Post buckling analysis must be conducted to analyze the panel under diagonal tension. Different theories are placed for this purpose [7], which can be summarized as follows

## ***II-4-2-a Theory of the Shear Buckling Resistant Panels:***


Fig. (29) Cross-sections of built up beams [7]

Figure (29) shows typical cross-sections of built-up beams of sufficiently thick webs to resist buckling up to the failing load (yielding). The beam is called in this case '*buckling resistant beam*'. If the web to flange connection is adequately stiff, the stresses in the built up beams follow fairly well the formulae of engineering theory of bending, where

$$\sigma = \frac{Mz}{I}$$
$$q = \frac{VQ}{I} \tag{45}$$

Where, 'M' and 'V' are the bending moment and the shear force respectively, 'Q' is the first moment of area of the area enclosed above the point of interest along the cross-section, 'I' is the second moment of inertia of the cross-section and 'z' is the distance from the point of interest to the neutral axis of the cross-section.
It is well known that the distribution of the shear flow along the depth of the web follows a parabolic distribution where the maximum value is located at the shear center, or at the neutral axis for symmetric webs.

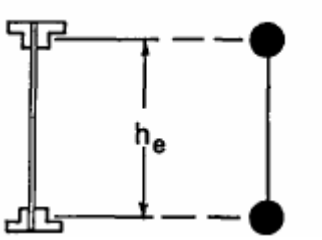


Fig. (30) Cross-section of the shear resistant 'Plate Girder' beam [7]

If the depth of the flange is small compared to the depth of the beam as shown in figure (30) the formulae for the design of the shear resistant panel beam can be simplified to what is called 'Plate Girder' equations,

$$\sigma_f = \frac{M}{h_e A_F}$$
$$q = \frac{V}{h_e} \tag{46}$$

Where '$A_f$' is the cross-section area of the flange.

Designing a heavily loaded rib to have a shear resistant panel will generate a massive structure. Accordingly, optimizing the wing box structure for a minimum mass objective function requires the design for a diagonal tension field state.

## ***II-4-2-b Theory of Pure Diagonal Tension:***

The theory of pure diagonal tension was developed by Wagner [8].

## ***Basic Concepts***

The diagonal tension beam is defined as a built-up beam similar in construction to the plate girder but with a web so thin that buckles into diagonal fields at a load well below the design load.

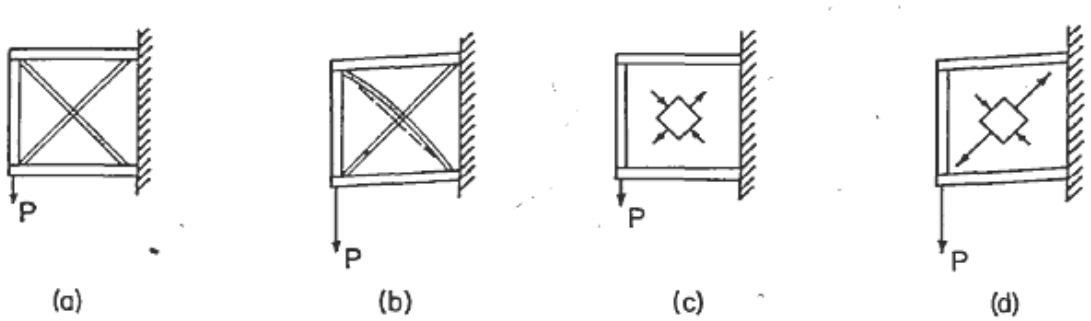


Fig. (31) Principle of diagonal tension [7]

Figure (31) shows a simple example to explain the full diagonal tension web. Figure (31-a) consists of a parallelogram frame of stiffness bars, hinged at the corners and braced internally by two slender diagonals of equal size. As long as the load 'P' is very small the two diagonals will carry equal and opposite stresses. at certain critical value of 'P' the compression diagonal will buckle as shown in figure (31-b) and thus loose its ability to take additional increments of stress. Consequently, if 'P' is increased further by large amount, the additional diagonal bracing force must be furnished mostly by the tension diagonal. At very high applied loads the stress in the tension diagonal will be so large that the stress in the compression diagonal is negligible by comparison.

As analogous, change in the state of stress will occur in a similar frame in which the internal bracing consists of a thin sheet, as shown in figure (31-c) at low values of the applied load, the sheet is in the state of pure shear, which is statically equivalent to equal tensile and compressive stresses at $45^{o}$ to the frame axes. At certain critical value of the load 'P' the sheet buckles as the load 'P' is

increased beyond the critical value, the tensile stresses become rapidly predominant over the compressive stress, as shown in figure (31-d). The buckles develop a regular pattern of diagonal folds, at an angle '$\alpha$' and following the lines of diagonal tensile stress. When the tensile stress is so large that the compressive stress can be neglected entirely by comparison the sheet is said in the state of 'fully developed' or 'pure diagonal tension'.

## ***Primary Stresses:***

To analyze the stresses in a web in pure diagonal tension, the web is assumed to be cut into a series of ribbons or strips of unity width, measured horizontally. Each strip is inclined at an angle '$\alpha$' to the horizontal axis and is under a uniform tensile stress. As shown in figure (32-a)

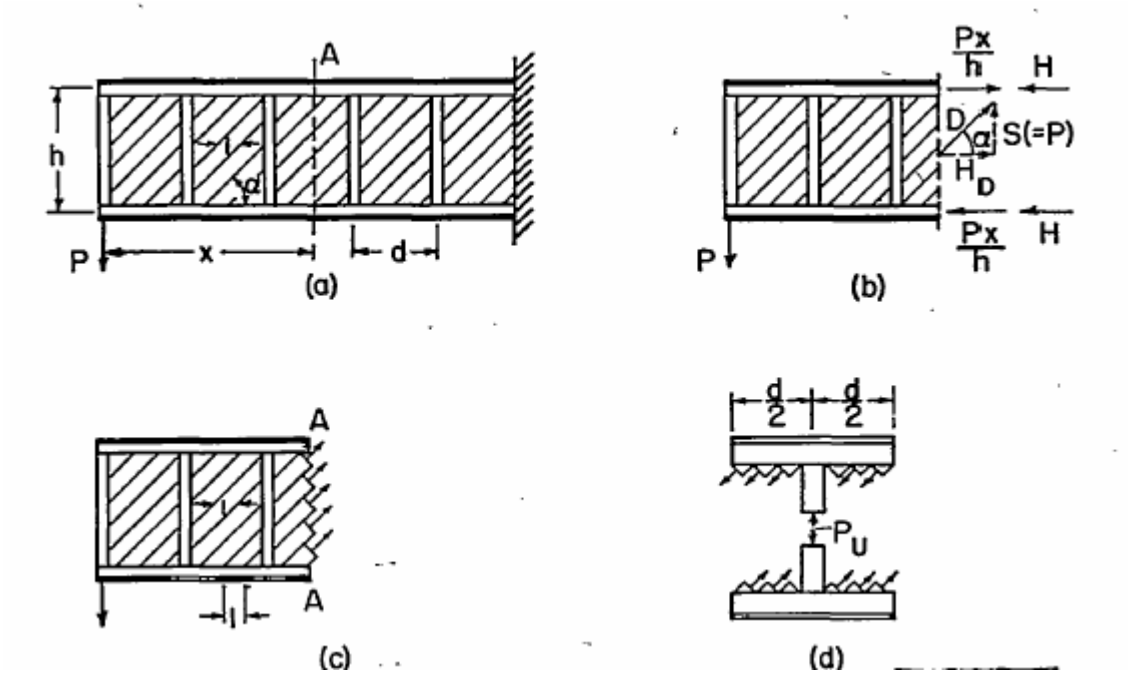


Fig. (32) Forces in Diagonal Tension Field Beam [7]

The free body diagram of Figure (32-b) shows the internal forces in the strips as the web is cut through section A-A, these internal forces are combined to their resultant 'D'. Since all strips have the same stress, the resultant is located at the mid-height. The horizontal component of this resultant force 'D' is

$$H_D = V\cot(\alpha) \tag{47}$$

This horizontal force is balanced by a two equal compressive force 'H' in the flanges, since the force 'D' is acting at the mid height

$$H = -\frac{V}{2}\cot(\alpha) \tag{48}$$

According to the idealized beam theory combined with the pure diagonal tension field theory, the total load in the flange will be

$$F = \pm\frac{M}{h} + H = \pm\frac{M}{h} - \frac{V}{2}\cot(\alpha) \tag{49}$$

From figure (32-d) it is clear that the diagonal tension strips are intending to pull the two flanges together. Accordingly, the existence of an upright is a must for the stability of the web; this upright will be under compression. The compressive force in the upright is equal to the vertical forces acting in the strips

$$P_U = -V\frac{d}{h}\tan(\alpha) \tag{50}$$

Where '$P_U$' is the compressive force in the upright and 'd' is the distance between two adjacent uprights. In case of using only one upright, then 'd' can be expressed as one half of the distance between the front and the rear spar.

All primary stresses calculated are function in the diagonal tension stress inclination angle 'α', where an expression is adopted for this angle as

$$\tan^4(\alpha) = \frac{1+\frac{ht}{2A_F}}{1+\frac{dt}{A_U}} \tag{51}$$

For practical use, the angle '$\alpha$' is assigned an average value of 44°.

The stresses in the flange and the upright can then be calculated, where

$$\begin{aligned} \sigma_F &= \frac{F}{A_F} = -\frac{\tau ht}{2A_F}\cot(\alpha) \\ \sigma_U &= \frac{P_U}{A_U} = -\frac{\tau dt}{A_U}\tan(\alpha) \end{aligned} \tag{52}$$

Where $A_U$ is the cross-section area of the upright.

It should be noted that the flange stress calculated in equation (52) is the stress generated due to the diagonal tension stresses. The effect of the bending stress in the plane of the web is not included in this form.

## ***Secondary Stresses:***

Due to the tension forces in the web strips, the upper and the lower flange will be subjected to bending stress, as a secondary stress, as well as the compressive primary stresses. In this case the flange can be considered as a continuous beam supported by the upright. The total bending load is equal to $P_U$, which is the total compressive force in the upright, but is distributed along the flange.

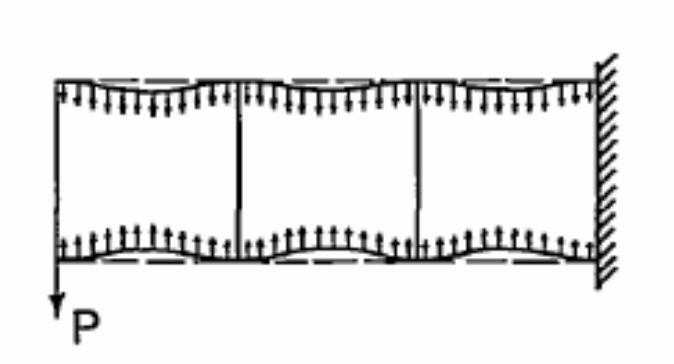


Fig. (33) Secondary bending stresses acting on the upper and the lower flange [7]

Figure (33) shows the strips tension forces which generate the secondary bending stress in the flange. Considering that this load is uniformly distributed, the maximum bending moment will be at the upright,

$$M_{\max} = \frac{Vd^2 \tan(\alpha)}{12h} \qquad (53)$$

It is important to indicate that the previous calculations are based on the assumption that the flange is stiff enough, that it will not bend excessively to release the tension field stresses in some strips, else a further analysis should be considered to the redistribution of stresses due to the excessive bending deformation of the flanges.

## ***Behavior of the Upright:***

The upright is a stiffener that is introduced to the web to oppose the tendency of the diagonal tension strips to pull the upper and the lower flanges together. It may be in the form of a stiffener member, double on both faces of the web or single on one side of the web both should be fastened to the web; or it may be a vertical bead in the web surface. In both cases and since it is subjected to compressive stress, a buckling analysis should be conducted to insure that it will be stable under the compressive load.

The traditional buckling analysis of columns can not be applied directly to the upright, since the upright is fastened into the web or a built-in part of the web as in the case of the vertical beads. But the analysis should be modified because once the upright starts buckling; it will be subjected to a distributed transversal load acted upon from the diagonal tension field strips, trying to turn it back into the plane of the web. The magnitude of this restoring load is proportional to the deflection of the upright. Wagner [9] introduced the curve shown in Figure (35) for the ratio of '$\frac{P_U}{P_{U_E}}$' as a function in the ratio of '$\frac{d}{h}$', where $\frac{P_U}{P_{U_E}}$ is the ratio of the buckling load of a double upright to Euler's buckling load (the buckling load in case the stiffeners are not fastened to the web) while the ratio $\frac{d}{h}$ is the ratio between the distance between two adjacent uprights to the height of the web.

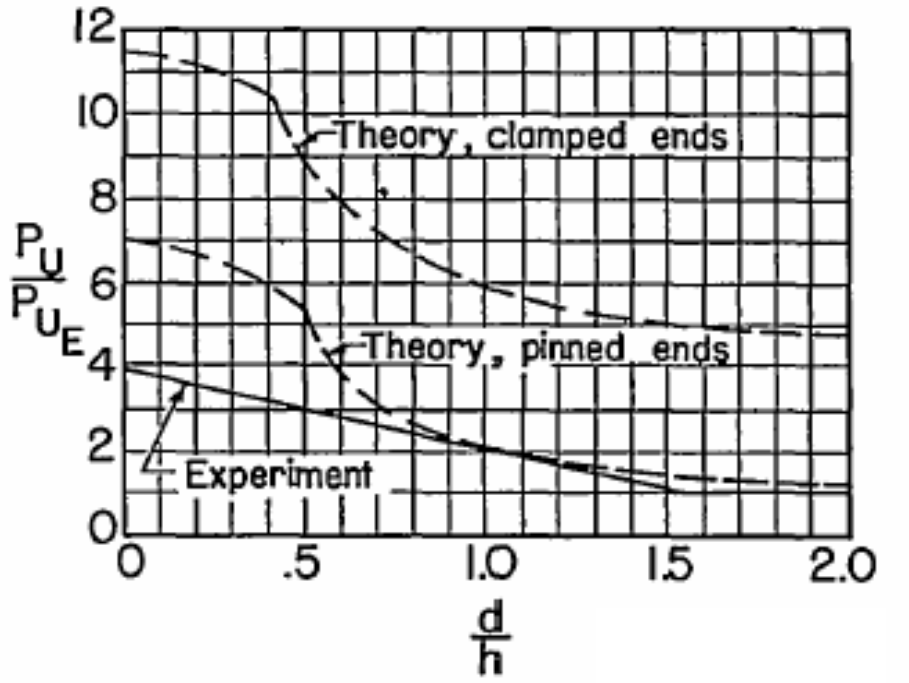


Fig. (35) Buckling loads of a double upright fastened into a flat web [7]

In the calculation of these curves Wagner made an assumption that the upright was clamped to the flange, which can not be obtained unless the flange would had an infinite torsional stiffness which is not the case in actual structures. Most designs are characterized by low torsional stiffness flanges. Accordingly the line denoted by experimental in figure (35) is slightly conservative and may be used to obtain results for the buckling analysis of the uprights.

Single uprights will be subjected to eccentric effect, because the centroid of the upright cross-section will be shifted from the plane of the web by a distance of eccentricity 'e' then the bending moment in the upright will be

$$M_{U_e} = eP_U \tag{54}$$

And the stress in the upright superficial fibers will be

$$\sigma_U = \frac{P_U}{A_U}\left(1+\left(\frac{e}{\rho}\right)^2\right) = \frac{P_U}{A_{U_e}} = -\frac{\pi dt}{A_{U_e}}\tan(\alpha) \tag{55}$$

Where $A_{U_e}$ is the effective area of the upright that can be expressed as

$$A_{U_e} = \frac{A_U}{1+\left(\frac{e}{\rho}\right)^2} \qquad (56)$$

And '$\rho$' is the upright cross-section radius of gyration of the area moment of inertia with respect to an axis parallel to the web surface.

It should be noted that in case of the double upright, the last two formulae can be used with 'e=0'.

## ***Stability of the Upright:***

### *(i) Failure by buckling instability*

As mentioned before, the upright is subjected to compressive stress. It is considered as a column in compression. Accordingly, it is subjected to column buckling instability, as previously discussed.

Recalling equation (36), the Euler's buckling load for an elastic column in compression can be expressed as $P_{cr} = n^2 \frac{\pi^2 E I_y}{a^2}$ , where 'n=1' presents the 1st mode of buckling. Accordingly, the term '$P_{U_E}$' in figure (35), can be expressed as

$$P_{U_E} = \frac{\pi^2 EI}{L_e{}^2} \qquad (57)$$

Where '$L_e$' is the effective length of the upright. The effective length of the upright is presented by an empirical formula in the form

$$L_e = \frac{h_U}{\sqrt{1+K^2\left(3-2\frac{d}{h_U}\right)}} \qquad for \quad (d < 1.5h)$$
$$L_e = h_U \qquad for \quad (d > 1.5h) \qquad (58)$$

Where 'K' is called diagonal tension factor (K=1 in the case of pure diagonal tension, further details for the diagonal tension factor will be presented in later sections) and '$h_U$' is the height of the upright. '$I$' in equation (57) is the second

moment of area of the upright cross-section with respect to an axis parallel to the web surface.

'I' can be expressed in the form $I = \rho^2 A_U$, where '$\rho$' is the upright cross-section radius of gyration. Accordingly, equation (57) can be rewritten as

$$P_{U_E} = \frac{\pi^2 E A_U}{\left(\frac{L_e}{\rho}\right)^2} \qquad \text{or} \qquad \sigma_{U_E} = \frac{P_{U_E}}{A_U} = \frac{\pi^2 E}{\left(\frac{L_e}{\rho}\right)^2} \tag{59}$$

The actual compressive load acting on the upright can be calculated using equation (52). Using equation (59) the Euler's buckling load can be calculated. With the help of figure (36), the critical buckling load for a double upright fastened to a plane web can be calculated. With comparison with the load applied on the upright, the stability of the upright can be checked.

For a conservative design, the standard Euler buckling curves can be used to obtain the allowable value of the stress in the upright '$\sigma_{U_{all}}$' with slenderness ratio '$\left(\frac{L_e}{\rho}\right)$'. Then the stability can be checked by checking that $\sigma_U \leq \sigma_{U\,all}$.

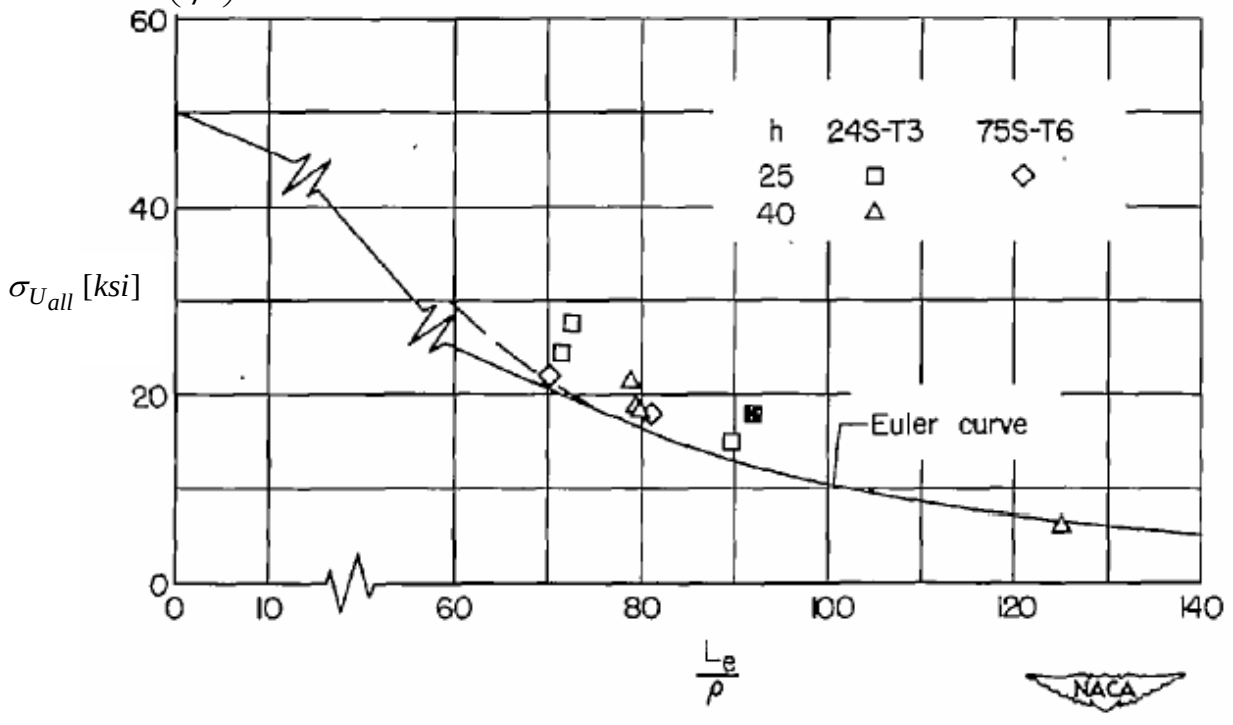


Fig. (35-a) Allowable compressive load in the upright [7]

### *(ii) forced crippling:*

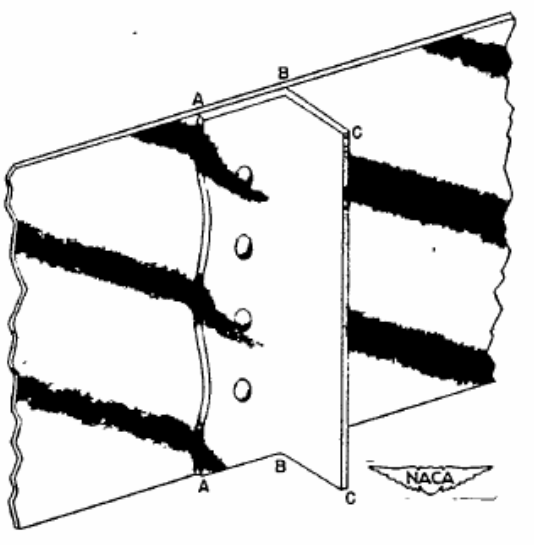


Fig. (36) Failure of the upright by forced crippling [7]

Figure (36) shows a section in a web under diagonal tension and reinforced by an upright. The shear buckles that take place in the web forces the upright to buckle along the edge A-A of the attachment leg. The amplitude of this wave is maximum along the free edge at A-A and zero along the corner B-B. If the deformations are large then some small waves would appear along the edge C-C. This leads us to the conclusion that not all the cross-section of the upright is sharing in the bending stiffness of the upright. To enable that the, the upright should be welded to the web along the line B-B but this is not the case in practice. The governing equations for this type of failure will be shown in the section of the allowable stresses.

## ***II-4-2-c Engineering Theory of Incomplete Diagonal Tension:***

When a gradually increasing load is applied to a beam with a plane shear web, at low loads the beam behaves in accordance to the shear resistant beam theory. At certain critical load value, the web buckles and an upright should be introduced to the web. As the load increases more and more, the buckles become deeper and the buckle pattern changes slowly to approach the well developed diagonal tension case.

It is very rare that the beam will remain in a shear resistant until failure, but the common is that it will buckle moving to the diagonal tension. On the other hand it is also very rare that the beam reaches the case of the complete diagonal tension without encountering any failure. Accordingly, it is clear that the two cases of the shear resistant and the complete diagonal tension are a limiting cases and the real practical case is the incomplete diagonal tension case.

Referring to figure (31), the Incomplete Diagonal Tension Theory can be stated as: As the load 'P' increases from zero, both diagonals work initially. At certain load value '$P_{cr}$', the compression diagonal will buckle, the load in the diagonal being '$D_{cr}$'. For any further increase in the load 'P' beyond its critical value, the load in the compression diagonal is assumed to be constant '$D_{cr}$'. In other words if the applied shear stress in the web '$\tau$' is larger than the its critical value '$\tau_{cr}$', only the excess shear stress ($\tau - \tau_{cr}$) will produce the diagonal tension effects.

$$\tau_{DT} = \tau - \tau_{cr} = \tau\left(1 - \frac{\tau_{cr}}{\tau}\right) \qquad (60)$$

Where '$\tau_{DT}$' is the excess portion of the shear stress that generate the diagonal tension case. It is important to note that the applied shear stress '$\tau$' is a nominal stress, i.e. it does not exist, but it is split into two parts

1) '$\tau_{DT}$' which is carried by diagonal tension action.

$$\tau_{DT} = K\tau \qquad (61)$$

'K' is called the 'Diagonal Tension Factor' where

$$K = 1 - \frac{\tau_{cr}}{\tau} \tag{62}$$

2) '$\tau_S$' which is carried by the true shear action of the web.

And $\tau_S = K\tau$ (63)

An empirical formula for the value of 'K' may be used to replace the previously calculated theoretical formulae, where the experiments showed that for '$1 < \frac{\tau}{\tau_{cr}} < 2$' the diagonal tension factor can be approximated by the formula

$$K = 0.434\left(\rho + \frac{1}{3}\rho^3\right) \tag{64}$$

Where $\rho = \frac{\tau - \tau_{cr}}{\tau + \tau_{cr}}$

For $\tau < \tau_{cr}$ the factor 'K' is considered zero, and the web is loaded in the shear resistant case. As the ratio $\tau/\tau_{cr}$ approaches infinity the diagonal tension factor approaches unity, and the web is said to be in the complete diagonal tension case.

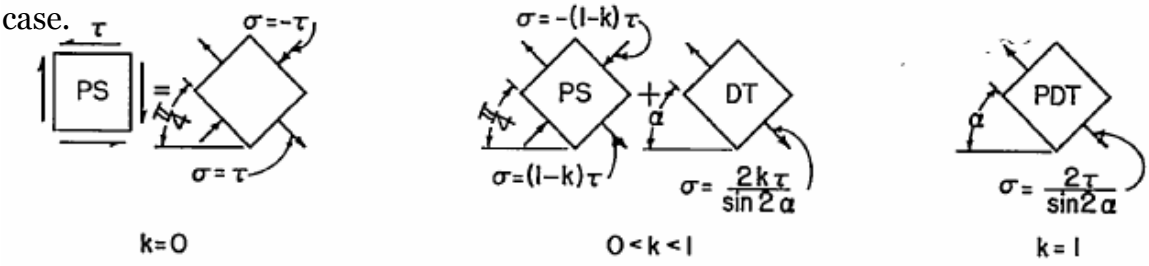


Fig. (37) Stress systems in diagonal tension webs [7]

Figure (37) shows the different stress cases for the shear webs. The intermediate case is showing the general case of the incomplete diagonal tension case, superimposing the stresses in this case, gives the stresses in the direction of 'α' denoted by '$\sigma_1$' and the stress in the perpendicular direction denoted by '$\sigma_2$'

$$\sigma_1 = \frac{2K\tau}{\sin(2\alpha)} + \tau(1-K)\sin(2\alpha), \qquad \sigma_2 = -\tau(1-K)\sin(2\alpha) \tag{65}$$

And since it is assumed that the web is carrying a part of the load as compressive load, so it is convenient to consider it supporting a part of the compressive load applied formerly to the upright. Accordingly, equation (52) can be modified to

$$\sigma_U = -\frac{K\tau\tan(\alpha)}{\frac{A_{U_e}}{dt}+0.5(1-K)}$$
$$\sigma_F = -\frac{K\tau\cot(\alpha)}{\frac{2A_F}{ht}+0.5(1-K)} \quad (66)$$

## ***II-4-2-d Failure of the web under the effect of the incomplete diagonal tension:***

The stress in the web can be expressed as a nominal shear stress. An empirical formula for the peak nominal stress in a flat panel is presented as

$$\tau'_{\max} = \tau\left(1+K^2C_1\right)\left(1+KC_2\right) \quad (67)$$

Where $C_1$ is a correction factor for the tolerance of the angle '$\alpha$' if it is slightly changed than its average value of '45°' and 'K' is the 'diagonal tension factor'

For 'K=1' (i.e. the complete diagonal tension case) the angle correction factor is calculated using the formula

$$C_1 = \frac{1}{\sin(2\alpha)} - 1 \quad (68)$$

For other values of 'K' the value of $C_1$ can be obtained from figure (38) based on the calculated value of the angle '$\alpha$'

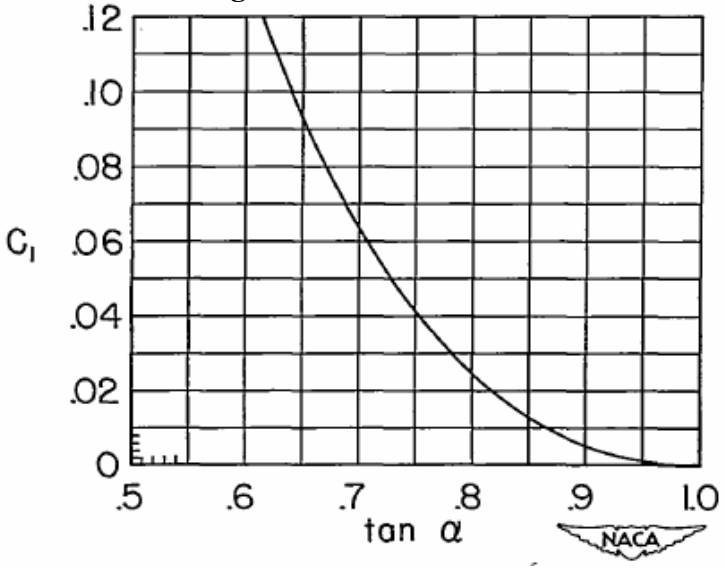


Fig. (38) Angle Factor $C_1$ [7]

'$C_2$' is the stress concentration factor arising from flexibility of the flanges. Which can be obtained from Figure (39)

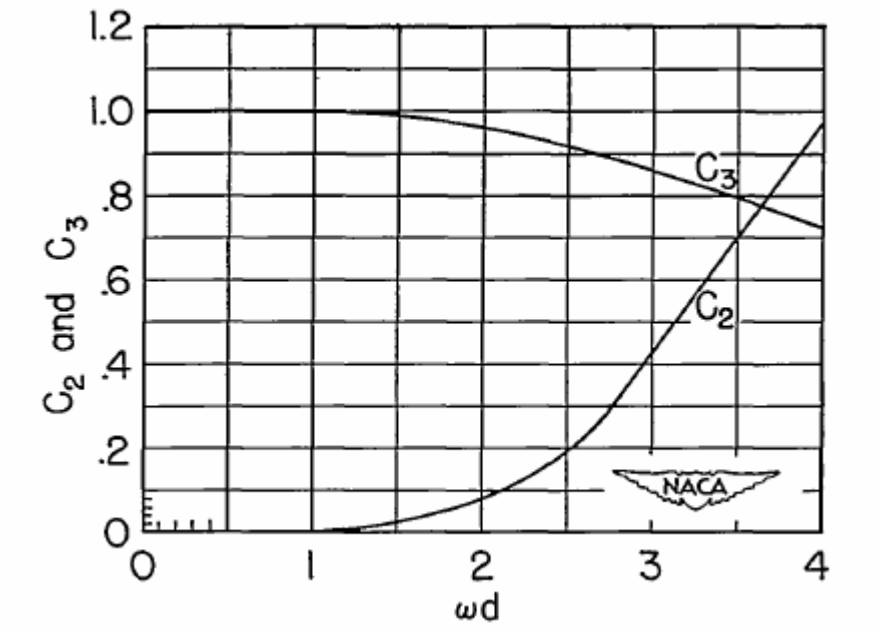


Fig. (39) Stress concentration factors $C_2$ and $C_3$ [7]

The horizontal axis in figure (39) represents the *flange-flexibility parameter* $\omega d$ which can be expressed as

$$\omega d = d\sin(\alpha)\sqrt[4]{\left(\frac{1}{I_T}+\frac{1}{I_C}\right)\frac{t}{4h}} \tag{69}$$

Where $I_T$ and $I_C$ represent the second moment of area of the tension and the compression flanges respectively (with respect to their centroidal axis).

## ***II-4-2-e Summary for the Stress Analysis of Flat Webs Under Diagonal Tension Filed:***

Based on what is mentioned in the previous sub-sections, the terms used in stress analyzing a flat web stressed in an incomplete diagonal tension can be summarized as

### ***(i) Effective area of the Upright:***

(1) For single Upright

$$A_{U_e} = \frac{A_U}{1+\left(\frac{e}{\rho}\right)^2} \qquad \text{(a)}$$

(2) For Double Symmetrical Upright

Put 'e=0' then

$$A_{U_e} = A_U \qquad \text{(b)}$$

An estimate for the value of $\frac{A_{U_e}}{A_U}$ can be made using the following figure

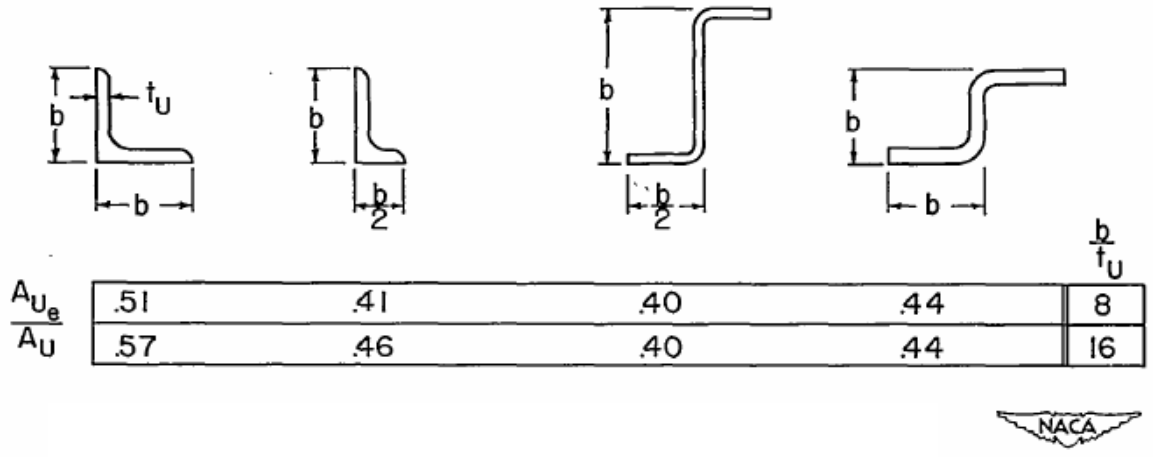


Fig. (41) Ratio of the effective to the actual area of the upright [7]

### ***(ii) Effective column length of the Upright:***

The effective column length '$L_e$' of an upright is given by the empirical formula

$$L_e = \frac{h_U}{\sqrt{1+K^2\left(3-2\frac{d}{h_U}\right)}} \qquad for \quad (d<1.5h)$$

$$L_e = h_U \qquad for \quad (d>1.5h) \tag{c}$$

Where '$h_U$' is the length of the upright.

### *(iii) Critical shear Stress:*

The critical shear stress in the web can be calculated using equation

$$\tau_{cr} = \eta_s C_s \frac{\pi^2 E}{12(1-\nu^2)}\left(\frac{t}{b}\right)^2 \tag{d}$$

Where 'b' in this equation represents the smaller dimension in the web, which will be its height in the case of the rib, then this equation, can be reformulated as

$$\tau_{cr} = \eta_s C_s \frac{\pi^2 E}{12(1-\nu^2)}\left(\frac{t}{h}\right)^2 \tag{e}$$

Where the shear constant $C_s$ can be obtained from figure (27).

### *(iv) Nominal Web Shear Stress:*

The nominal web shear stress can be calculated using the formula

$$\tau = \frac{q_{\max}}{t} \tag{f}$$

Where '$q_{\max}$' is the maximum shear flow in the web.

### *(v) Diagonal Tension Factor:*

The diagonal tension factor can be calculated based on the stress ratio '$\frac{\tau}{\tau_{cr}}$',

for '$1<\frac{\tau}{\tau_{cr}}<2$' $\qquad K = 0.434\left(\rho+\frac{1}{3}\rho^3\right)$ (g)

Where $\rho = \frac{\tau-\tau_{cr}}{\tau+\tau_{cr}}$ For $\tau < \tau_{cr}$ the factor 'K' is considered zero

### *(vi)* ***Angle of Incomplete Diagonal Tension:***

For practical use, the angle '$\alpha$' is approximated by '44°'. Also, an empirical figure based on experimental results is introduced for the calculation of this angle

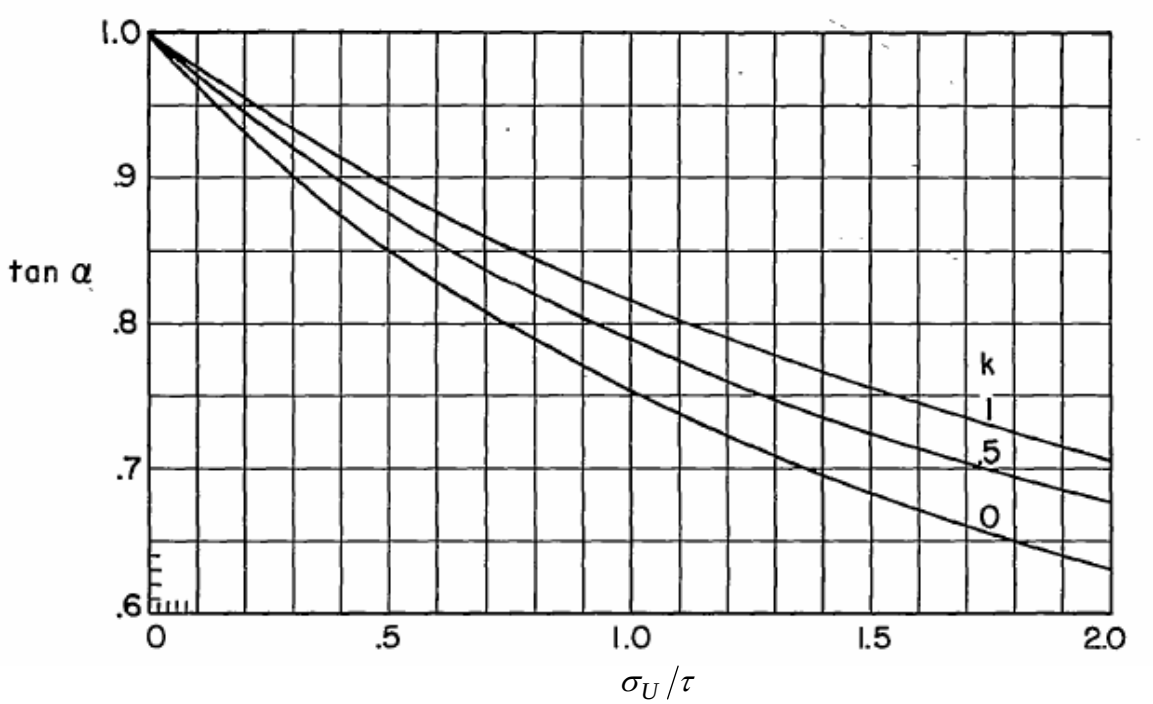


Fig. (42) Angle of the incomplete diagonal tension [7]

### *(vii)* ***Stresses in the Upright:***

The stress in the upright can be calculated using the formula

$$\sigma_U = -\frac{K\tau\tan(\alpha)}{\frac{A_{U_e}}{dt} + 0.5(1-K)} \tag{h}$$

It is important to note that the value of $\sigma_U$ calculated here is the average compressive stress along the upright, but the maximum value always takes place at the mid-height of the upright.

The ratio $\frac{\sigma_{U_{\max}}}{\sigma_U}$ can be obtained empirically, using the following curve

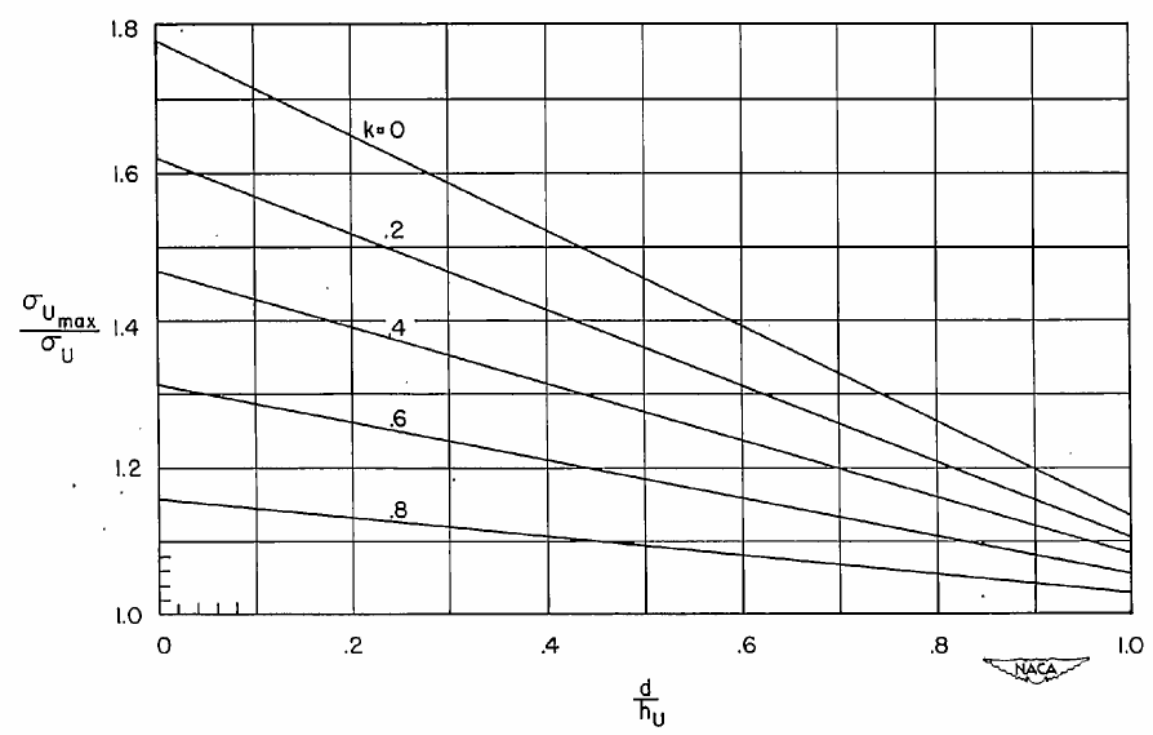


Fig. (43) Ratio of the maximum stress to the average stress in the upright [7]

It is important to note that the calculation of the upright stress is dependent on the incomplete diagonal tension angle, while to obtain the angle using the curve presented in figure (42), the stress in the upright is required. Accordingly, the angle is given an initial value of '44°' which is used for the calculation for the stress in the upright, then an iteration process is conducted to estimate the approximate value of the angle with sufficient convergence (normally, three iterations are enough to obtain the approximate value).

***(viii) <u>Maximum web stress:</u>***

The maximum stress in the web can be calculated as

$$\tau'_{\max} = \tau\left(1 + K^2 C_1\right)\left(1 + KC_2\right) \qquad \text{(i)}$$

Where $C_1$ can be obtained from figure (38). While the value of $C_2$ can be obtained from figure (39).

## ***II-4-2-f Allowable Stresses:***

### *(i) Allowable web stress:*

An empirical curves based on experimental results are designed for the calculation of the allowable stresses in plane shear webs. The experiments showed that failure in webs always starts at the web-to-flange attachment line. Although the shear stress through out the whole web should be investigated, but in most cases the web-to-flange attachment line would be the line of maximum stress. The experiments were done for samples made of 24S-T3 Aluminum alloy with ultimate strength of '62 ksi' and 75S-T6 Aluminum alloy with ultimate strength of '72 ksi'. Figures (44) and (45) show the results.

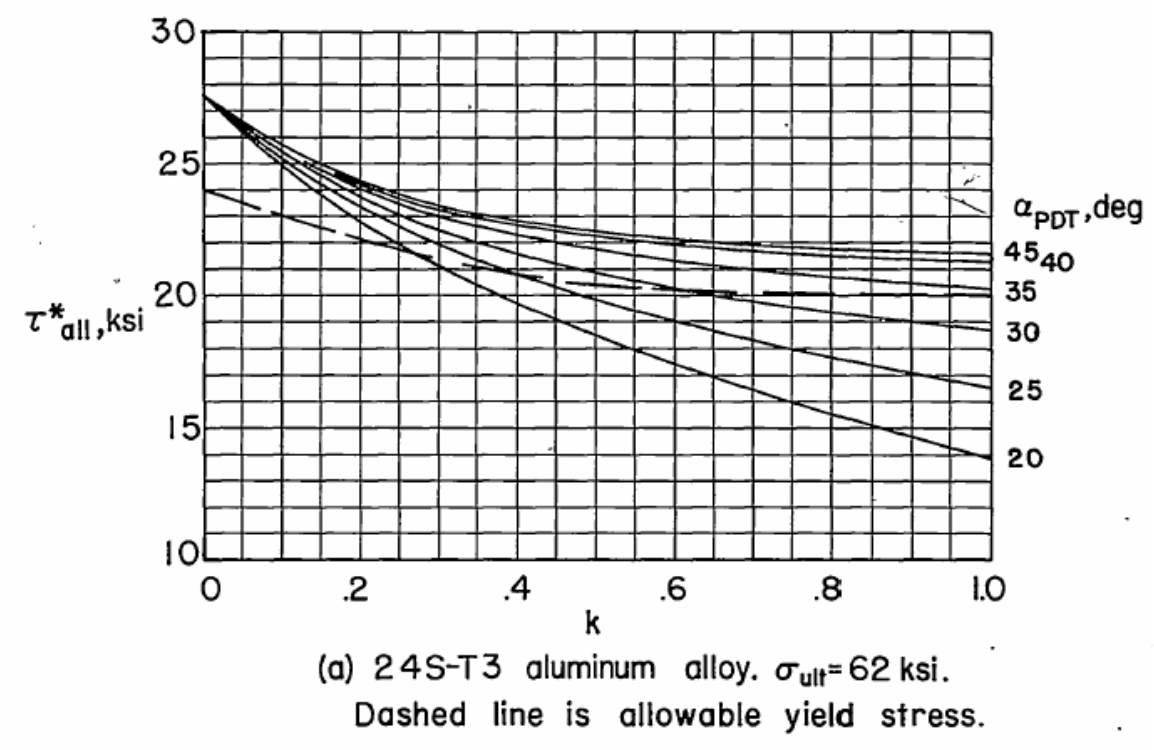


Fig. (44) Allowable value of maximum shear stress in the web [7]

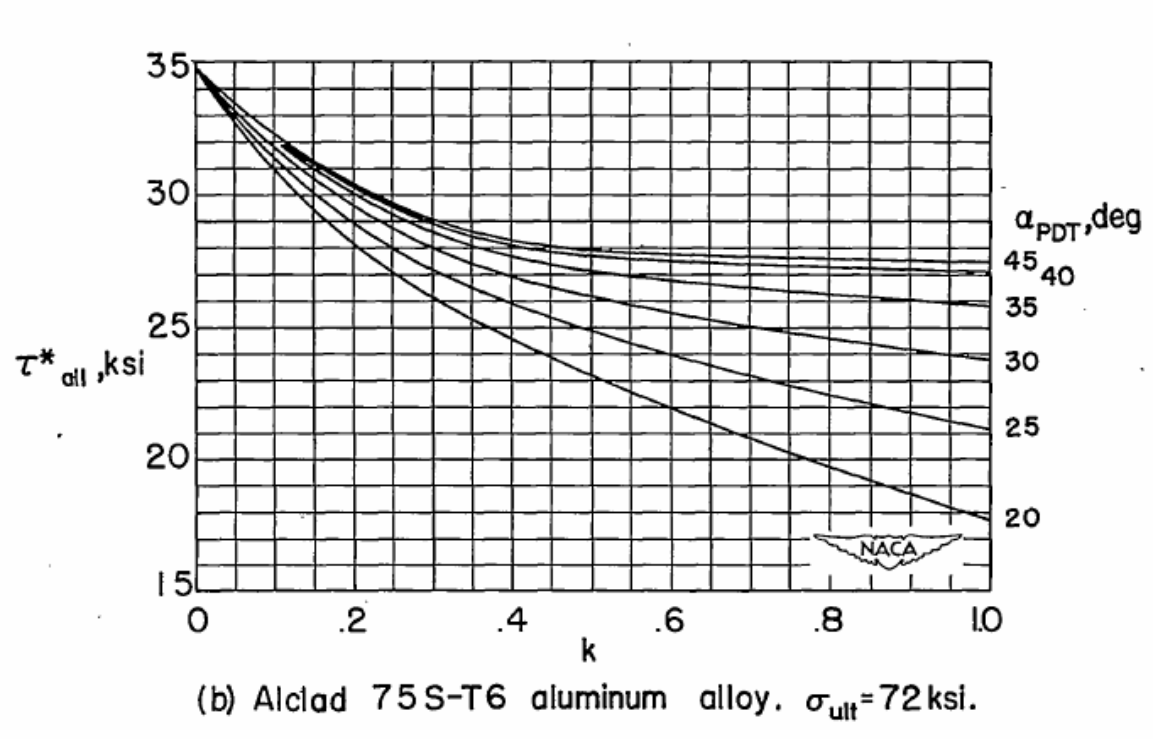


Fig. (45) Allowable value of maximum shear stress in the web [7]

In Figures (44) and (45) the allowable value of the shear stress can be determined based on the 'K', the diagonal tension factor, and '$\alpha_{PDT}$', angle of Pure Diagonal Tensions. As mentioned before, this angle can be computed using equation (51) or for practical use, the line in the figure (44) and (45) corresponding to angle $45^{o}$ can be used.

***(ii) <u>Allowable stress in the uprights:</u>***

Uprights are subjected to two types of failure namely the 'forced crippling failure' and the "column action failure" or buckling instability. To avoid upright failure, the limiting values of the stresses must be considered.

(a) allowable stresses for double (symmetrical) uprights

- to avoid forced crippling failure:

The maximum upright stress '$\sigma_{U_{\max}}$' should not exceed the allowable value '$\sigma_0$' defined by the following formula

$$\sigma_0 = 21K^{\frac{2}{3}}\left(\frac{t_U}{t}\right)^{\frac{1}{3}} \quad [ksi] \qquad for\ (24S-T3\ \ alloy)$$
$$\sigma_0 = 26K^{\frac{2}{3}}\left(\frac{t_U}{t}\right)^{\frac{1}{3}} \quad [ksi] \qquad for\ (75S-T6\ \ alloy) \qquad \text{(j)}$$

- To avoid column failure or buckling instability:

The allowable or the critical buckling stress in the upright can be obtained using figure (35-a) with slenderness ratio $\left(\frac{L_e}{\rho}\right)$ while the actual load in the upright can be obtained using equation (h). To avoid buckling, the actual load value must not exceed the critical buckling load.

(b) allowable stresses for single uprights

- to avoid forced crippling failure:

  The maximum upright stress '$\sigma_{U_{\max}}$' should not exceed the allowable value '$\sigma_0$' defined the following empirical formula

$$\sigma_0 = 26K^{\frac{2}{3}}\left(\frac{t_U}{t}\right)^{\frac{1}{3}} \quad [ksi] \qquad for\ (24S-T3\ \ alloy)$$
$$\sigma_0 = 32.5K^{\frac{2}{3}}\left(\frac{t_U}{t}\right)^{\frac{1}{3}} \quad [ksi] \qquad for\ (75S-T6\ \ alloy) \qquad \text{(k)}$$

- to avoid column failure or buckling instability:

  The average stress in the upright should not exceed its allowable value obtained from figure (35-a). The average stress can be calculated using equation (h) with consideration to the effective area of the single upright.

# Section III Wing Rib Design Procedure

Ribs can be classified according to its type of loading. For example, a Rib subjected only to aerodynamic loads is always considered as a lightly loaded rib while a rib subjected to concentrated forces transferred to its structural from fuel tanks supporting points, control surfaces supporting points (flaps, ailerons…etc), armament supporting points…etc is considered a moderately loaded rib. A heavily loaded rib which is always referred to a bulkhead is a one subjected to concentrated forces transferred to its structure from landing gears and power plant nacelles supporting points.

The design procedure of the wing rib depends mainly on its type of loading as well as some constraints that should be satisfied in the design process like the requirements of cut outs for the inspection holes and wiring and piping passages though the wing…etc.

Although the ideal design for the wing rib is designing for incomplete diagonal tension state which is efficient from the point of view of weight saving but sometimes the existence of cut outs prevent the design for the diagonal tension case.

In this section, two design methodologies for the wing rib will be discussed.

## III-1 The 1st Method: Shear Resistant Plate Girder:

This design method is suitable for lightly loaded ribs and sometimes for moderately loaded ribs with cut outs.

In this method the wing rib will be designed as a shear resistant plate girder that will not buckle nor yield under the applied loads. It may not be practical to think about designing a lightly loaded rib as a diagonal tension beam, although it will result in a reduced thickness web that will be advantageous from the point of view of weight reduction. But this merit can be restored by omitting web stiffeners and, instead, introducing a series of standard flanged lightening holes in to the web, as shown in the following figure

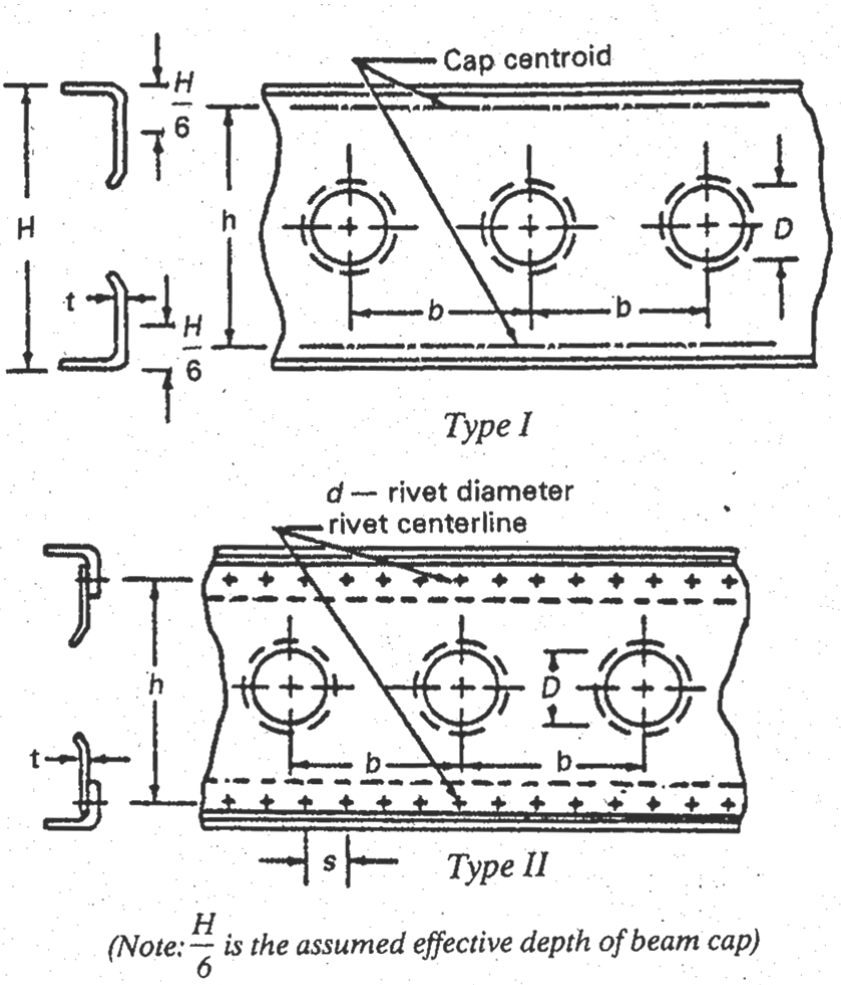


Fig. (46) Lightly loaded rib with standard flanged lightening holes [12]

There are two types of standard flanged lightening holes

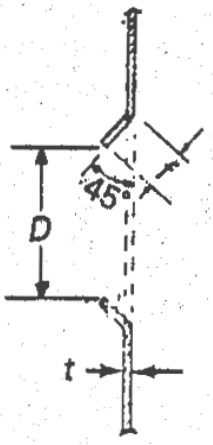


| D (inch) | 2.0 | 2.5 | 3.0 | 3.5 | 4.0 | 4.5 | 5.0 | 6.0 |
|---|---|---|---|---|---|---|---|---|
| f (inch) | .25 | .3 | .4 | .45 | .5 | .5 | .5 | .55 |

Fig. (47) Lightening holes of typical flanged (45° flanged) [12]

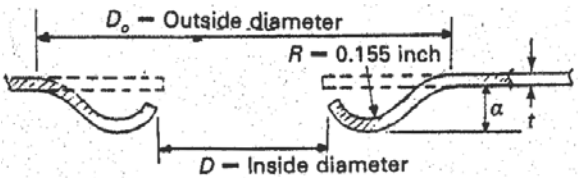


| $D_0$ (Inch) | $D$ (Inch) | $\alpha$ (Inch) |
|---|---|---|
| 1.7 | 0.8 | 0.2 |
| 1.95 | 1.05 | 0.2 |
| 2.65 | 1.7 | 0.25 |
| 3.0 | 2.05 | 0.25 |
| 3.65 | 2.7 | 0.25 |
| 3.9 | 2.95 | 0.25 |
| 4.95 | 3.8 | 0.4 |
| 5.95 | 4.8 | 0.4 |
| 6.95 | 5.8 | 0.4 |
| 7.44 | 6.3 | 0.4 |
| 7.95 | 6.8 | 0.4 |
| 8.95 | 7.8 | 0.4 |
| 9.45 | 8.3 | 0.4 |

Fig. (48) Lightening holes with beaded flanged [12]

The design curves for aluminum alloy webs with flanged holes are shown in the next figure

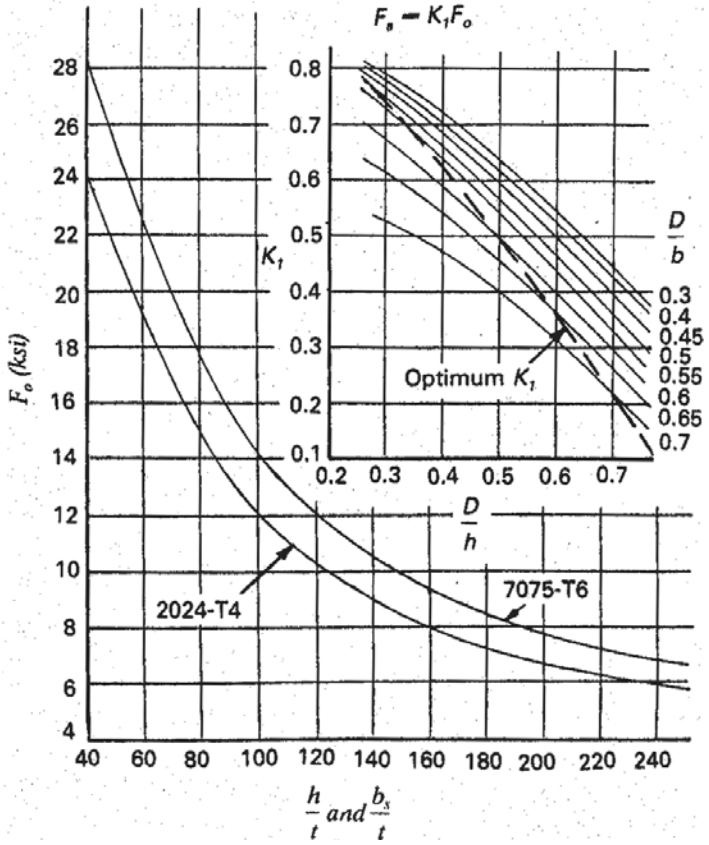


Fig. (49) Ultimate allowable gross shear stress for aluminum alloy webs with flanged holes [12]

Where D…the inner diameter of the hole

h…the height of the web

t…thickness of the web

b…distance between the center of two adjacent holes

The limiting conditions that must be satisfied to use the design curves shown in figure (49) are

$$0.25 \le \frac{D}{h} \le 0.75 \tag{1.1}$$

$$0.016 \le t \le 0.125 \tag{1.2}$$

$$0.3 \le \frac{D}{b} \le 0.7 \tag{1.3}$$

$$40 \le \frac{h}{t} \le 250 \tag{1.4}$$

As shown in figure (49), the value of the ultimate allowable gross shear stress is

$$F_s = K_1 F_o \tag{1.5}$$

Where $F_o$…ultimate allowable shear stress for web without holes

$F_s$… ultimate allowable gross shear stress in the web

$K_1$…correlation factor.

In case of large holes, then the net shear stress in webs between holes and shear stress in vertical sections across the holes should be calculated and assured that it is less than the gross shear stress.

The net shear stress in webs between the holes

$$f_s = \frac{q}{t}\left(\frac{h}{h-D}\right) \tag{1.6}$$

While the net shear stress in the vertical section across the hole is

$$f_s = \frac{q}{t}\left(\frac{b}{b-D}\right) \tag{1.7}$$

The value of the stress calculated in equations (1.6) and (1.7) must be less than the value of the stress '$F_s$' obtained from figure (49).

**The steps of the 1st design method can be summarized as:**

(1) Load Calculation:

At the wing station where the wing rib is located, the aerodynamic loads will be determined in the form of pitching moment, bending moment and shear force. These loads will be used to calculate the shear flow around the airfoil cross-section. This shear flow will be applied directly to the perimeter of the wing rib.

(2) Maximum shear flow '$q_{max}$' calculation:

Based on the shear flow distribution, calculated in the previous step, the Shear flow through out the wing rib cross-sections will be calculated to determine the value of the maximum shear flow. In case of aerodynamic loads which are transferred to the rib from the skin-stringer panels, the maximum shear flow is always located at the rib perimeter.

(3) Determination of the geometrical constraints:

According to the wing box cross-section dimensions at the specified spanwise wing station, the values of the wing maximum section height '$H$' and width $C_r$ (the distance between the front and the rear spar) will be obtained. From figure (46), if the wing rib is of the first type (I) where the web cap is an integral part of the web, then the height of the web can be calculated as '$h = \frac{2}{3}H$' where '$\frac{1}{3}H$' is stored for the effective depth of the upper and the lower integrated web cap. The trailing and leading edge rib parts will not be considered in the current analysis.

(4) According to the wing rib material type, the modulus of elasticity, yield strength in tension, compression and shear, ultimate strength and Poisson's ratio will be specified.

(5) Based on the shear flow calculations, the maximum shear stress will be calculated in terms of the wing rib thickness 't'.

$$\tau_{max} = \frac{q_{max}}{t} \tag{1.8}$$

(6) The value of the critical buckling shear stress will be calculated using the formula

$$\tau_{cr} = \eta_s C \frac{\pi^2 E}{12(1-\nu^2)}\left(\frac{t}{h}\right)^2 \quad (1.9)$$

In this equation, the value of the constant 'C' will be obtained from Figure (27) based on the following parameters

(i) Boundary conditions

The rib is considered as simply supported from all sides.

(ii) Aspect ration

The horizontal axis in figure (27) represents the web aspect ratio where

$$\frac{a}{b} = \frac{C_r}{h} \quad (1.10)$$

(7) To avoid wing rib web buckling under the current loading, the maximum shear stress in the rib must not exceed the value of the critical buckling shear stress where

$$\tau_{\max} \leq \tau_{cr} \quad (1.11)$$

Based on the previous inequality, the minimum value of the wing rib web thickness can be obtained as

$$t = \sqrt[3]{\frac{12\left(1-\nu^2\right)}{\eta_s \pi^2 E}\left(\frac{h^2 q_{\max}}{C}\right)} \quad (1.12)$$

In equation (1.12) the value of the plasticity coefficient '$\eta_s$' will be considered equal to one since the rib is being designed for pure elastic conditions.

(7) Now, the value of the maximum shear stress $\tau_{\max}$ based on the calculated web thickness in the previous step will be calculated and compared with the value of the yield shear stress of the wing rib material. If $\tau_{\max} < \tau_y$ , then the value of the web thickness obtained is right. Else, the value of '$\eta_s$' must be calculated and entered to equation (1.12) for recalculation of web thickness.

(8) The weight of the wing rib can be calculated as

$$W_R = A_{rj} t \rho_R g \quad (1.13)$$

where '$\rho_R$' is the specific mass of the wing rib material, 'g' is the gravity acceleration and $A_{rj}$ is the wing rib area at station 'j' along the wing span. The

value of the weight will be useful to compare the results of the different design methodology.

(9) Based on the web thickness calculated in the previous step and the web height calculated in the 3rd step, equations (1.2) and (1.4) will be used to check the rib limiting conditions for the use of the lightening holes design curves.

(10) Once the dimensions satisfy the limiting conditions, then the maximum net shear stress in the web can be calculated as $f_s = \frac{q_{\max}}{t}$ because no lightening holes are introduced yet.

(11) Using the design curves in figure (49) with the value of '$\frac{h}{t}$' then the value of the ultimate allowable shear stress for the web without holes '$F_o$' can be obtained.

(12) Using equation (1.5) along with the values of '$F_o$' and $F_s = f_s$, then the value of the correlation factor '$K_1$' can be calculated.

(13) Again using the design curves presented in figure (49) along with the value of '$K_1$' and using the optimum '$K_1$' curve, then we can get values for the ratios '$\frac{D}{h}$' and '$\frac{D}{b}$'. Using these two ratios, then the diameter of the lightening holes can be calculated.

(14) Using figures (47) and (48) to select a standard hole's diameter based on the choice between beaded flanged hole or typical flanged hole with 45° flanged.

(15) Based on the standard diameter for the hole obtained in the previous step, the ratio '$\frac{D}{h}$' should be recalculated. Then with the new ratio of '$\frac{D}{h}$' along with the value of '$K_1$' calculated in step (12) and using figure (49) a new ratio for '$\frac{D}{b}$' can be obtained then the holes spacing 'b' can be calculated.

(15) Now, the value of the allowable shear flow can be calculated as

$$q_{all} = K_1 F_o t \qquad (1.14)$$

(16) Margin of safety check:

Using equation (1.6) and (1.7) the net shear stress in the web between the holes and in the vertical section passing through the hole must be calculated. Check that

$$M.S. = \left( \frac{\max(f_s)}{q_{all}} - 1 \right) \geq 0 \tag{1.15}$$

If this inequality is satisfied then the design is safe.

(17) Based on the width of the rib '$C_r$', the diameter of the lightening holes 'D' and the holes spacing 'b' the number of lightening holes in the rib can be calculated as

$$n_h = \frac{C_r}{b} - 1 \tag{1.16}$$

The value obtained from equation (1.16) should be rounded to the smaller integer $n_{hr}$.

(18) Then based on the rounded number of holes the actual hole spacing can be computed as

$$b_r = \frac{C_r}{n_{hr} + 1} \tag{1.17}$$

## ***III-2 The 2nd Method: Incomplete Diagonal Tension Shear web:***

(1) Assume the value of the web thickness obtained in the previous method is '$t_1$'

(2) At web thickness '$t_1$', the web is acting as a 'plate girder' that will not buckle nor yield under the current loading.

(3) Assume '$t_2$' to be the thickness of the web at which the material starts yielding which can be calculated as

$$t_2 = \frac{q_{\max}}{\tau_y} \tag{2.1}$$

(4) based on the values of '$t_1$' and '$t_2$' a new web thickness value 't' will be suggested as an input value for the design process of the wing rib, where

$$t = t_2 + \left( \frac{t_1 - t_2}{2} \right) \tag{2.2}$$

(5) For sure at this web thickness the web will buckle, and it will be considered in the case of incomplete diagonal tension state of stress.

(6) Based on the input value of 't', the nominal shear stress in the web can be calculated as

$$\tau = \frac{q_{\max}}{t} \tag{2.3}$$

(7) Based on the value of 't', calculate the value of the critical buckling stress

$$\tau_{cr} = \eta_s C \frac{\pi^2 E}{12(1-\nu^2)} \left( \frac{t}{h} \right)^2 \tag{2.4}$$

Note that $\eta_s = 1$ because the whole design process is considered to be taking place in the elastic zone of stress and the value of 'C' can be obtained from figure (27).

(8) Since the web is in the incomplete diagonal tension state of stress, uprights must be introduced into the web. It is always advisable to reduce the distance between the adjacent uprights in order to reduce the flexibility of the flanges which is necessary to eliminate the secondary stresses arising from the non-uniform distribution of the diagonal tension stress along the web due to excessive deformation of the flange. It is recommended to consider '$d \approx h$' where 'd' is the distance between adjacent uprights while 'h' is considered as two third the of the airfoil thickness because one third of the airfoil thickness is always assumed for the upper and lower rib cabs.

Based on that the number of uprights that should be included in the design can be calculated as

$$n_U = \frac{C_r}{h} \tag{2.5}$$

Where the value of '$n_U$' will be rounded to the nearest integer.

(9) the distance between the adjacent uprights can be calculated using the rounded value of '$n_U$' as

$$d = \frac{C_r}{n_U} \tag{2.6}$$

Where '$C_r$' is the distance between the front and the rear spars.

(10) Based on the value of nominal shear stress '$\tau$' and the critical buckling stress '$\tau_{cr}$' that are calculated in steps (6) and (7) respectively, the diagonal tension factor 'K' can be calculated using the empirical formula

For '$1 < \frac{\tau}{\tau_{cr}} < 2$'

$$K = 0.434\left(\rho + \frac{1}{3}\rho^3\right) \qquad \text{Where} \qquad \rho = \frac{\tau - \tau_{cr}}{\tau + \tau_{cr}} \tag{2.7}$$

For $\tau < \tau_{cr}$ the factor 'K' is considered zero

**(11) Designing the uprights:**

Assume that the single upright construction will be selected for the design process where one stiffener will be fastened to the web.

The upright is subjected to two types of failure

**a) Column Failure or buckling instability:**

To avoid column failure the average value of the stress in the upright should not exceed its allowable or its critical buckling stress which can be obtained using figure (35-a) with slenderness ratio $\left(\frac{L_e}{\rho}\right)$ where '$L_e$' is the effective length of the upright, which can be calculated as

$$L_e = \frac{h_U}{\sqrt{1 + K^2\left(3 - 2\frac{d}{h_U}\right)}} \qquad for \quad (d < 1.5h) \tag{2.8}$$

$$L_e = h_U \qquad for \quad (d > 1.5h)$$

To compute the radius of gyration, the geometry of the upright cross-section should be defined first.

To find the shape of the upright cross-section, figure (41) is showing different types of upright cross-sections, selecting the angle type with equal legs length, and selecting the ratio of $\frac{b}{t_U} = 8$, the ratio of $\frac{A_{U_E}}{A_U} = 0.51$

$$\frac{A_{U_E}}{A_U} = \frac{1}{1+\left(\frac{e}{\rho}\right)^2} = 0.51 \qquad (2.9)$$

Assuming that the upright leg normal to the plane of the web is the effective part in resisting the buckling failure then

$$e = \left(\frac{b+t}{2}\right) \qquad (2.10)$$

Substituting equation (2.10) into equation (2.9) the value of 'b' can be computed. Refer to figure (41) for specifying the dimension 'b'.

Since $\frac{b}{t_U} = 8$, then the thickness of the upright can be computed, then the cross-section area of the upright can be computed as

$$A_U = 2bt_U - t_U^2 \qquad (2.11)$$

Then the second moment of area with respect to an axis passing through the centroid of the web cross-section and parallel to the plane of the web can be calculated as

$$I = \frac{1}{12}t_U b^3 + bt_U\left(\frac{b+t_U}{2}\right)^2 = A_U\rho^2 = \left(2bt_U - t_U^2\right)\rho^2 \qquad (2.12)$$

Using equation (2.12) the radius of gyration of the upright cross-section can be computed.

Then the ratio of $\left(\frac{L_e}{\rho}\right)$ can be calculated, then figure (35-a) can be used to find the allowable value for the buckling load in the upright.

**a) Forced crippling failure (local buckling):**

To avoid the forced crippling, the maximum stress in the upright should not exceed its allowable value,

$$\sigma_{\max} \le \sigma_0 = 26K^{\frac{2}{3}}\left(\frac{t_U}{t}\right)^{\frac{1}{3}} \quad [ksi] \qquad for\ (24S-T3\ Allu\min um\ alloy)$$
$$\sigma_{\max} \le \sigma_0 = 32.5K^{\frac{2}{3}}\left(\frac{t_U}{t}\right)^{\frac{1}{3}} \quad [ksi] \qquad for\ (75S-T6\ Allu\min um\ alloy) \tag{2.13}$$

The maximum stress in the upright can be calculated using the figure (43) while the average stress in the upright can be calculated using the equation

$$\sigma_U = -\frac{K\tau\tan(\alpha)}{\frac{A_{U_e}}{dt}+0.5(1-K)} \tag{2.14}$$

Based on the calculated dimensions for the upright, its effective area can be calculated. Then the average stress in the upright can be calculated

Then the ratio $\sigma_U/\tau$ can be calculated, using this ratio with figure (41) a new value for the diagonal tension angle can be obtained.

Based on the new value of the diagonal tension angle, the average stress in the upright can be recalculated.

Repeat the previous two steps in an iteration process until we reach an acceptable convergence for the value of the angle $\alpha$.

With the value of $\frac{d}{h}=\frac{d}{h_U}$ and the diagonal tension factor 'K', use figure (42) to obtain the ratio of $\frac{\sigma_{U_{\max}}}{\sigma_U}$, then the maximum stress in the upright can be calculated.

Check for $\sigma_{U_{\max}} < \sigma_o$

(12) Checking for web failure:

The maximum shear stress in the web can be calculated using the equation

$$\tau'_{\max} = \tau\left(1+K^2C_1\right)\left(1+KC_2\right) \tag{2.15}$$

Where $$C_1 = \frac{1}{\sin(2\alpha)} - 1$$

While the value of $C_2$ can be obtained from figure (39).

From figure (42) the value of the allowable shear stress in the web can be obtained $\tau^{*}_{all}$ .

Check for $\tau'_{\max} < \tau^{*}_{all}$ (2.16)

# References

[1] http://aaac.larc.nasa.gov/tsab/cfdlarc/aiaa-dpw, 3rd AIAA CFD Drag Prediction Workshop, San Francisco, 2006

[2] Kuhn P, Stresses in Aircraft and shell structures, McGraw-Hill Book Company, 1956

[3] Bruhn E.F, Analysis and Design of Flight Vehicle Structures, Jacobs & Associates Inc., June 1973

[4] Airplane stress analysis, NACA report No. 82.

[5] M. Abdo, P. Piperni, F. Kafyeke "Conceptual Design of Stinger Stiffened Compression Panels".

[6] Gerard, G. and Becker, H. 'Hand Book of Structural Stability (Buckling of Compression Elements)' NACA TN 3782.

[7] Paul Kuhn, James P. Peterson and Langely Field, Technical Note 2661, 'A Summary of Diagonal Tension Field' Part-I, Method of Analysis, Washington May1952.

[8] Wagner, Herbert; 'Flat Sheet Metal Girders with Very Thin Metal Web'. Part I- General Theories and Assumptions. NACA TM 604, 1931.

[9] Wagner, H., and Ballerstedt, W. "Tension Fields in Originally Curved, This Sheets During Shearing Stresses". NACA TM 774, 1935.

[10] Wagner, H. "Remarks on Airplane Struts and Girders Under Compressive and Bending Stresses". Index Values. NACA TM 500, 1929.

[11] Howard D. Curtis, 'Fundamentals of Aircraft Structural Analysis', WCB McGraw-Hill, 1997.

[12] Niu M, Airframe Stress Analysis and Sizing, Conmilit Press Ltd., 1997.